

# Restricted location of PSEN2 $\gamma$ -secretase determines substrate specificity and generates an intracellular A $\beta$ pool

Ragna Sannerud<sup>a,b</sup>, Cary Esselens<sup>a,b</sup>, Paulina Ejsmont<sup>a,b</sup>, Rafael Mattera<sup>c</sup>, Leila Rochin<sup>d,e</sup>, Arun Kumar Tharkeshwar<sup>a,b</sup>, Greet De Baets<sup>f,g</sup>, Veerle De Wever<sup>g</sup>, Roger Habets<sup>h</sup>, Veerle Baert<sup>a,b</sup>, Wendy Vermeire<sup>a,b</sup>, Christine Michiels<sup>a,b</sup>, Arjan J. Groot<sup>h</sup>, Rosanne Wouters<sup>a,b</sup>, Katleen Dillen<sup>a,b</sup>, Katlijn Vints<sup>i</sup>, Pieter Baatsen<sup>i</sup>, Sebastian Munck<sup>i</sup>, Rita Derua<sup>g</sup>, Etienne Waelkens<sup>g</sup>, Guriqbal S. Basil<sup>i</sup>, Mark Mercken<sup>k</sup>, Marc Vooijs<sup>h</sup>, Mathieu Bollen<sup>g</sup>, Joost Schymkowitz<sup>f,g</sup>, Frederic Rousseau<sup>f,g</sup>, Juan S. Bonifacino<sup>c</sup>, Guillaume Van Niel<sup>d,e</sup>, Bart De Strooper<sup>a,b,l</sup>, and Wim Annaert<sup>a,b</sup>

a, Center for the Biology of Disease, VIB & b, Dept of Human Genetics, KU Leuven, Belgium

c, Cell Biology & Neurobiology Branch, NICHD, NIH, Bethesda, MD, USA

d, Institut Curie, PSL Research University & e, CNRS, UMR 144, Paris, France

f, Switch Laboratory-VIB & g, Dept of Cell & Mol Medicine, KU Leuven, Belgium

h, Dept. of Radiotherapy (MAASTRO)/GROW, Maastricht University, The Netherlands

i, BioImaging Core-VIB, Leuven, Belgium

j, Avalanche Biotechnology, Menlo Park, CA, USA

k, Janssen Pharmaceutica, Beerse, Belgium

l, Dept of Molecular Neuroscience, UCL Institute of Neurology, London, UK

Correspondence: [wim.annaert@cme.vib-kuleuven.be](mailto:wim.annaert@cme.vib-kuleuven.be)

## Summary

$\gamma$ -Secretases are a family of intramembrane cleaving proteases involved in various signaling pathways and diseases, including Alzheimer's disease (AD). Cells co-express differing complexes, including two homologous presenilins (PSEN). We examined the biological relevance of this heterogeneity and identified a unique motif in PSEN2 that directs this  $\gamma$ -secretase to late endosomes/lysosomes via a phosphorylation-dependent interaction with the AP-1 adaptor complex. Accordingly, PSEN2 selectively cleaves late endosomal/lysosomal localized substrates and generates the prominent pool of intracellular A $\beta$  that contains longer A $\beta$ ; familial AD (FAD)-associated mutations in PSEN2 increased the levels of longer A $\beta$  further. Moreover, a subset of FAD mutants in PSEN1, normally more broadly distributed in the cell, phenocopies PSEN2 and shifts its localization to late endosomes/lysosomes. Thus, localization of  $\gamma$ -secretases determines substrate specificity while FAD-causing mutations strongly enhance accumulation of aggregation-prone A $\beta$ 42 in intracellular acidic compartments. The findings reveal potentially important roles for specific intracellular, localized reactions contributing to AD-pathogenesis.

## Introduction

$\gamma$ -Secretases constitute a family of biologically and pathologically relevant intramembrane cleaving proteases (i-Clips) (Jurisch-Yaksi et al., 2013; Wolfe, 2009). They consist of four subunits and are structurally very different from other i-Clips such as the rhomboids (Freeman, 2014) and signal peptide peptidases (SPPs & SPPLs) (Voss et al., 2013), which are monomeric or dimeric proteins. The catalytic activity of the complex is provided by the PSEN1 or PSEN2 subunit isoforms, while three additional subunits, APH1A or B/C, nicastrin (NCT), and PEN-2 are needed to build a functional enzyme (De Strooper and Annaert, 2010; Edbauer et al., 2003; Takasugi et al., 2003). Thus, and disregarding alternative splicing of PSEN and APH1 subunits, at least four distinct  $\gamma$ -secretase complexes can coexist in the same cell (De Strooper and Annaert, 2010). To date, it is unclear why cells express so many different  $\gamma$ -secretases, since overexpression studies suggest that the different complexes can cleave the same substrates, and mutations in both *PSEN* genes can cause Alzheimer's disease (AD). On the other hand, murine knockouts of different subunits show major phenotypical differences suggesting biologically diverse functions (Jurisch-Yaksi et al., 2013; Serneels et al., 2005). For instance, PSEN1 or APH1A knockout mice show severe embryonic phenotypes due to deficient Notch signaling, while PSEN2 or APH1B/C knockout mice display a normal life span (Serneels et al., 2005). Biochemical evidence also suggests that the four different  $\gamma$ -secretase complexes process the Amyloid Precursor Protein (APP) differently, generating shorter or longer A $\beta$  peptides depending on the subunit composition (Acx et al., 2014).

Other i-Clips make use of the compartmentalization of the cell to control cleavage of their various substrates (Freeman, 2014; Golde et al., 2009; Krawitz et al., 2005). However, it is remarkable how little is known about the subcellular compartmentalization of  $\gamma$ -secretase complexes (De Strooper and Annaert, 2010). Here, we used a variety of approaches to establish that two major  $\gamma$ -secretase classes, comprising PSEN1 and PSEN2 as alternative subunits, have very different subcellular locations. We identify a motif in PSEN2 that restricts its location to late endosomes/lysosomes (LE/LYS) and interacts specifically and in a phosphorylation-dependent manner with the trans-Golgi network (TGN)/endosomal adaptor complex protein (AP) complex AP-1 (Bonifacino, 2014). This more restricted localization of PSEN2 is conserved in a wide range of cell lines, in primary neurons, and in brain. PSEN1, instead, is

more broadly distributed in the cell, including the plasma membrane. This distinct distribution explains the differential preference for substrates of PSEN1- *versus* PSEN2-complexes. In addition, we find that PSEN2 produces a distinct intracellular pool of A $\beta$  that has been inferred to be pathological relevant, but whose origin was never precisely determined (Friedrich et al., 2010; Gouras et al., 2010; Pensalfini et al., 2014). Moreover, familial AD (FAD) mutations in PSEN2 strongly increase intracellular aggregation-prone A $\beta$ 42 production, and some FAD-PSEN1 mutations phenocopy FAD-PSEN2 with respect to localization, substrate specificity and intracellular A $\beta$ 42/40 ratio.

## Results

### **PSEN2/ $\gamma$ -secretase is restricted to late endosomes and lysosomes.**

To analyze the intracellular distribution of PSEN1 and PSEN2, we fractionated a postnuclear supernatant of wild-type (WT) mouse embryonic fibroblasts (MEFs) by discontinuous sucrose/D<sub>2</sub>O gradient centrifugation. PSEN1 immunoreactivity broadly distributed in all fractions whereas PSEN2 displayed a strong enrichment in fractions containing the LE/LYS markers Rab7 and Cathepsin D. The different fractions all contained active  $\gamma$ -secretase, as demonstrated by de novo A $\beta$  production using an *in vitro*  $\gamma$ -secretase assay (Figures 1A and 1A'). Magnetic isolation of LE/LYS using superparamagnetic iron oxide nanoparticles (SPIONs) confirmed that PSEN2, but not PSEN1, co-enriched with Rab7 and LAMP1 (Figure 1B). Finally, cell surface biotinylation of WT MEFs revealed a significant level of PSEN1 ( $9\% \pm 2.8$ , n=4) at the cell surface whereas PSEN2 was barely detected ( $1\% \pm 0.8$ , n=3) (Figures 1C and 1C'). Similar results were obtained with several independent cell lines, underscoring a broad conservation of the distinct distribution of PSEN1 and PSEN2 (Figures 1D and 1E).

We further confirmed the restricted localization of PSEN2 using confocal microscopy. The higher expression of PSEN2 in HEK293, MNT-1 and A549 cells (Figure S1A) allowed us to demonstrate the enrichment of endogenous PSEN2 in LAMP1 positive LE/LYS (Figure 1F). Also in murine primary hippocampal neurons (Figure 1G) and in brain tissue (Figure 1H), endogenous PSEN2 strongly co-localized with LAMP1, particularly in somatodendritic compartments. Because of the unavailability of antibodies that detect low levels of endogenous PSEN1 and in order to generate a cell model to study transport regulation, we engineered N-terminally fluorescent protein (GFP or TagRFP)-tagged PSEN1 and PSEN2 constructs and retrovirally expressed them in PSEN1 and PSEN2 single and double knockout (dKO) MEFs. We selected cell lines that expressed physiological (i.e., stoichiometric to other  $\gamma$ -secretase subunits) levels of PSENs, as demonstrated by endoproteolysis of GFP-PSEN, mature N-glycosylation of NCT, PEN-2 stabilization and processing of APP-CTF, the direct substrate of  $\gamma$ -secretase (Figure 1I). Of note, NCT was more abundant (1.7 fold) at the cell surface in PSEN1- versus PSEN2-rescued dKO MEFs (Figures 1J and 1J'), confirming the presence of PSEN1 complexes at the cell surface. GFP-PSEN2 was as expected mainly restricted to LAMP1-positive LE/LYS compartments (Figure 1K). Similar patterns were observed when PSEN1 and PSEN2 were rescued in single knockout

MEFs. GFP-PSEN1 co-localized with the ER-marker BIP and with transferrin receptor at the cell surface (Figure S1B), and GFP-PSEN2 with LAMP1 (Figure S1C). We also co-expressed both PSENs in dKO MEFs with identical results, implying that the overall localization of one PSEN is not influenced by the other (Figures S1B to S1D). Moreover, analysis of isolated plasma membrane sheets of GFP-PSEN1- and TagRFP-PSEN2-rescued dKO MEF lines confirmed the higher level of PSEN1 and the sparse presence of PSEN2 at the cell surface (Figure S1E). GFP-PSEN1 was as well more abundant in cell surface biotinylated fractions while GFP-PSEN2 co-purified with LAMP1 in LE/LYS isolates (Figures 1J, 1J' and S1F). Finally, when expressed in primary hippocampal neurons, GFP-PSEN2, but not GFP-PSEN1, localized to LysoTracker-positive compartments (Figure 1L), confirming that the tagged-PSENs behave as their endogenous counterparts also in neurons.

### **The N-terminus of PSEN2 contains a unique acidic-dileucine sorting motif**

We hypothesized that the restricted localization of PSEN2 complexes might be the consequence of a specific sorting motif. Transmembrane domains (TMDs) are highly conserved between PSEN1 and PSEN2 while the cytosolic N-terminus and loop between TMD6 and 7 are highly divergent. We swapped these domains between the PSENs (Figure 2A) and stably expressed the hybrid proteins in dKO MEFs. We found that all hybrids rescued  $\gamma$ -secretase maturation and activity (Figure 2B). However, whereas the cytosolic loop swap (hybrids 2 and 3) did not alter PSEN1 localization, the exchange of its N-terminus with the one of PSEN2 (hybrid 4) was sufficient to direct PSEN1 to LE/LYS, as shown by co-localization with LAMP1 (Figures 2C and C'). Conversely, replacing the N-terminus of PSEN2 by that of PSEN1 (hybrid 5) resulted in a WT PSEN1-like distribution. Thus, crucial sorting information is located within amino acids 1-76 of PSEN2.

Inspection of the PSEN2 N-terminal segment revealed a highly conserved E<sub>16</sub>RTSLM<sub>21</sub> sequence (Figure 3A), which fits the acidic-dileucine motif [D/E]xxxL[L/I/M] present in other proteins that are transported to LE/LYS (Traub and Bonifacino, 2013). This motif is known to bind to the heterotetrameric AP complexes AP-1, AP-2 and AP-3, which sort cargo at different stages of the endomembrane system. To determine whether the PSEN2 motif binds to these complexes, we first used a yeast 3-hybrid (Y3H) assay (Mattera et al., 2011) (Figure 3B, 3C). We found that the PSEN2 N-terminus interacted with the

AP-1  $\gamma$ - $\sigma$ 1, but not the AP-2  $\alpha$ - $\sigma$ 2 and AP-3  $\delta$ - $\sigma$ 3, hemicomplexes (Figure 3C). This interaction was lost when essential amino acids in the PSEN2 motif (Glu<sub>16</sub>, Leu<sub>20</sub>-Met<sub>21</sub> or combinations of them) were mutated to Ala (Figure 3C, 3D). Interestingly, interaction with the AP-2 hemicomplex was detected only when Met<sub>21</sub> was substituted by Leu (Figure S2A), indicating that the C-terminal –LM configuration of the motif is responsible for its selective binding to AP-1.

We next performed pull-down experiments from rat brain extracts using GST fused to the PSEN N-termini and again observed selective co-isolation of endogenous AP-1 only with GST-N<sub>1-86</sub>PSEN2, as detected by immunoblotting for the  $\gamma$  subunit (AP1G1) (Figure 3E). This interaction was not seen when critical residues in the PSEN2 motif were mutated to Ala (Figures 3F top). Finally, co-immunoprecipitation from extracts of cell lines expressing higher endogenous PSEN2 levels (Figure S1A), also confirmed interaction with AP-1 (Figure S2B).

### **Phosphorylation of the E<sub>16</sub>RTSLM<sub>21</sub> motif regulates PSEN2 interaction with AP-1**

Intriguingly Ser<sub>19</sub> in the E<sub>16</sub>RTSLM<sub>21</sub> sorting motif (Figure 3A) has been shown to undergo phosphorylation *in vivo* (Walter et al., 1996). We mutated this residue, and also two other conserved proximal serines (Ser<sub>7</sub> and Ser<sub>9</sub>) in GST-N<sub>1-86</sub>PSEN2 to a non-phosphorylatable Ala or a phosphomimetic Asp. Mutation of Ser<sub>19</sub> to Asp (S<sub>19</sub>D) but not Ala (S<sub>19</sub>A) abrogated AP-1 interaction in Y3H (Figure 3D) and GST pull-down assays (Figure 3F lower panel), suggesting that the interaction of PSEN2 with AP-1 is regulated by Ser<sub>19</sub> phosphorylation. In contrast, the other mutations did not affect interaction, again confirming the specificity of the effects of the Ser<sub>19</sub> mutation. We then tested the physiological importance of these interactions in intact dKO cells stably expressing GFP-PSEN2 WT or the AxxxAA, S<sub>19</sub>A, and S<sub>19</sub>D mutants. All constructs were expressed at physiological levels as shown by the restoration of  $\gamma$ -secretase assembly and activity (Figure S2C). In line with Y3H and GST pull-down experiments, co-immunoprecipitation analysis showed that AP-1 binds to PSEN2 WT and PSEN2-S<sub>19</sub>A, but not to PSEN2-AxxxAA and only weakly to PSEN2-S<sub>19</sub>D (Figures 3G-G'). Note that under these conditions, significantly more endogenous AP-1 bound to PSEN2-S<sub>19</sub>A, indicating a stronger interaction.

The canonical [D/E]xxxL[L/I/M] motif binds to AP-1 through interaction of the C-terminal L[L/I/M] residues with  $\sigma$ 1 (AP1S1) and through the N-terminal D/E residues with  $\gamma$  (AP1G1), as shown by

structural and biochemical analysis (Jia et al., 2014; Kelly et al., 2008; Mattera et al., 2011). Based on the available crystal structure of AP-1 (Jia et al., 2014) we calculated the interaction energies ( $\Delta\Delta G$  values in kcal.mol<sup>-1</sup>) for the different mutant *versus* WT PSEN2 motifs using FoldX forcefield (Figure 3I). We obtained high positive  $\Delta\Delta G$ -values when substituting Leu<sub>20</sub>-Met<sub>21</sub> and Glu<sub>16</sub> residues to Ala, consistent with their critical importance for the binding of the PSEN2 motif to the groove of the  $\sigma$ 1 and  $\gamma$ 1 subunits, respectively (Figure 3H). In this analysis, the S<sub>19</sub>D mutation or the addition of a phosphate to Ser<sub>19</sub> (ERT<sub>p</sub>S<sub>19</sub>LM) also disfavored the interaction by more than 1.5 kcal.mol<sup>-1</sup> (Figure 3I) as a result of non-optimal hydrogen-bonding and electrostatic interactions with the surrounding residues in the  $\sigma$ 1 subunit. Several mutations at this position are predicted to be detrimental for the interaction in particular - and next to Asp- Glu, which is as well phosphomimetic, and the structurally related Asn (D, E and N in Figure S2D).

Although casein kinase 1 (CK1) was previously suggested to phosphorylate Ser<sub>19</sub> (Walter et al., 1996), this was not confirmed by a kinase-substrate predicting algorithm (scansite3.mit.edu). Instead, Aurora A appeared to be a more likely candidate to phosphorylate Ser<sub>19</sub> while Ser<sub>9</sub> was predicted to be a CK2 site. To explore this prediction we performed *in vitro* kinase assays using recombinant kinases and either GST or GST-N<sub>1-86</sub>PSEN2 as substrates (Figure 3J). These data conclusively demonstrated that Ser<sub>19</sub> is preferentially phosphorylated by Aurora A and also confirmed the phosphorylation of Ser<sub>7</sub>/Ser<sub>9</sub> by CK2. The direct phosphorylation of Ser<sub>19</sub> by Aurora A was furthermore confirmed by MS/MS analysis of *in vitro* phosphorylated trypsin digested GST-N<sub>1-86</sub>PSEN2 (Figure S2E). Taken together, these data strongly support the phosphorylation-regulated interaction of PSEN2 with AP-1.

### **The E<sub>16</sub>RTSLM<sub>21</sub> motif regulates the targeting of PSEN2 to LE/LYS**

We next assessed the effect of different E<sub>16</sub>RTSLM<sub>21</sub> mutations on the localization of GFP-PSEN2 to LE/LYS. The phosphomimetic GFP-PSEN2-S<sub>19</sub>D mutant co-localized less well with LAMP1 than did WT PSEN-2 (Figure 4A and 4A'). The sorting mutant GFP-PSEN2-AxxxAA displayed an even lower co-localization with LAMP1 and exhibited a broad distribution resembling that of GFP-PSEN1 (Figure 1K). In accordance, using cell surface biotinylation, GFP-PSEN2-AxxxAA was, like GFP-PSEN1 (Figure 1J'), more abundantly localized at the plasma membrane (Figures 4B and B'). Interestingly, in



primary hippocampal neurons, AP-1 regulates sorting of receptors, such as the transferrin receptor, to the somatodendritic domain (Farias et al., 2012). Using specific axonal and dendritic markers, we measured the polarity index of PSEN2 in neurons. This clearly showed that GFP-PSEN2 is exclusively present in the somatodendritic compartment, while GFP-PSEN1 localizes to both axons and dendrites (Figures 4C and 4C'). Interestingly, GFP-PSEN2-AxxxAA exhibited a non-polarized distribution, indeed suggesting that AP-1 sorts PSEN2 to somatodendritic LE/LYS in neurons (Figure 4C'). Altogether these results further validate the role of AP-1 in the sorting and localization of PSEN2.

Intriguingly, the non-phosphorylatable GFP-PSEN2-S<sub>19</sub>A, accumulated not only in LE/LYS but also prominently in the TGN, as shown by the co-localization with TGN46 (Figure 4D) and AP-1 (Figure 4E). Occasionally, co-localization could be observed over long tubules emanating from the TGN (Figure 4E, inset). To further support the TGN localization of GFP-PSEN2-S<sub>19</sub>A, we co-expressed LAMP1-mCherry and correlated 2-color structured illumination microscopy imaging with electron microscopy (SIM-CLEM). GFP-PSEN2 WT is mainly localized to the limiting membrane of LAMP1-positive organelles that could be identified at the ultrastructural level as LE/MVBs and lysosomes (Figure 4F and 4F'). In contrast, GFP-PSEN2-S<sub>19</sub>A localized additionally to a juxtannuclear area (Figure 4G) that at the EM level associated with tubular structures and vesicles of the TGN, as evidenced by the presence of clathrin coats and their close vicinity to Golgi stacks (<500nm,(Peden et al., 2004)) (Figure 4G'; and Movie S1 and S2 using 2-color SIM-CLEM with LAMP1-mCherry and MitoTracker, respectively).

The above results suggest that AP-1 plays a role in sorting PSEN2 from the TGN to LE/LYS, although this role may not necessarily involve direct delivery but rather routing via endosomal compartments (Brulke and Bonifacino, 2009; Saftig and Klumperman, 2009). To test the involvement of early endosomes (EE) in this routing, we overexpressed Rab5Q79L, a GTP-locked mutant blocking transport from EE. GFP-PSEN2, but not GFP-PSEN1, readily accumulated in enlarged endosomes under these conditions (Figure S3A). Moreover, overexpression of Rab11, which causes cargo to accumulate in recycling endosomes, resulted in trapping of GFP-PSEN1, but not GFP-PSEN2, in this compartment (Figure S3B). Under the same conditions, GFP-PSEN2 AxxxAA, but not the non-phosphorylatable S<sub>19</sub>A mutant, co-localized with overexpressed Rab11 (Figure S3B). Overall, these data

indicate that the interaction with AP-1 directs PSEN2 via EE to LE/LYS while PSEN1 traffics through the Rab11 recycling compartment likely en route to the cell surface.

### **The subcellular localization of PSENs affects substrate specificity**

We wondered whether the different subcellular localization of PSEN1- and PSEN2- $\gamma$ -secretases could provide a basis for substrate specificity. Among candidate substrates that localize to LE/LYS, two proteins involved in the biogenesis of melanosomes (a type of lysosome-related organelle), tyrosinase-related protein (TRP1) and premelanosome protein (PMEL) (Wang et al., 2006; Watt et al., 2013). Indeed, confocal microscopy showed localization of endogenous PSEN2 to LAMP1-positive LE/LYS in MNT-1, a human melanocyte cell line (Rapooso and Marks, 2007) (57% overlap, Figure 1F), while exogenous PMEL co-localized with GFP-PSEN2 in rescued dKO MEFs (Figure S4A), conclusively demonstrating that substrate and enzyme are present within the same organelles.

We next used siRNA to silence PSEN1 or PSEN2 expression in MNT-1 cells. Knockdown of PSENs did not affect the overall maturation of PMEL or TRP1 (Figure S4B). However, the  $\gamma$ -secretase cleavage products PMEL-CTF and TRP1-CTF accumulated dramatically in PSEN2 knockdown MNT-1 cells while only a moderate effect was seen in PSEN1 knockdown cells (Figure 5A and 5A'). Similar results were obtained with single PSEN1- or PSEN2-knockout MNT-1 cells generated by CRISPR/Cas9 genome editing (Figure 5C). Of note, the knockout cell lines showed accumulation of APP-CTF demonstrating that APP can be processed by either one of the PSENs (Figure S4C). The physiological relevance of PSEN2-catalyzed cleavage was evident from further EM analysis showing that the maturation of melanosomes was impaired in PSEN2 knockdown and knockout cells (Figures 5B, 5D, 5D'), along with a sharp decrease of stage III and IV mature melanosomes and accumulation of stage II immature melanosomes (Watt et al., 2013). Finally, melanosomes in retinal pigment epithelium (RPE) of *Psen2*<sup>-/-</sup> mice appeared significantly rounder, less numerous, and surrounded by an enlarged limiting membrane (Figure S4D). These data indicated that PSEN2-selective substrate processing is required for proper melanosome maturation both in culture cells and in mice.

We next analyzed the distribution of more ubiquitously expressed substrates such as APP, N-cadherin and Notch. APP and Notch are distributed in intracellular compartments, and are also present

at the cell surface (Perez et al., 1999; Sannerud and Annaert, 2009; Tagami et al., 2008), while N-cadherin mainly resides at the cell surface (De Strooper and Annaert, 2010). We isolated crude membrane fractions in the absence of detergent, reasoning that under these conditions the different  $\gamma$ -secretases would only cleave substrates that are in the same membrane compartment *in vitro*. We analyzed membranes isolated from cells expressing only GFP-PSEN1 or -PSEN2, or from the different cell lines expressing sorting mutants. Cell surface expressed N-cadherin-CTF was less efficiently cleaved by PSEN2/ $\gamma$ -secretase than by PSEN1/ $\gamma$ -secretase (Figure 5E and 5E'). Swapping of the sorting motif between PSEN1 and PSEN2 (hybrids 4 & 5, respectively, Figure 2A) largely reversed this preference. Expression of the other sorting mutants confirmed this observation. GFP-PSEN2-S<sub>19</sub>A, which is restricted to TGN & LE/LYS failed to process N-cadherin while GFP-PSEN2-AxxxAA showed increased N-cadherin-cleavage (Figures 5F and 5F'), reminiscent of WT PSEN1. APP-CTF was processed to the APP-intracellular domain fragment (AICD) to similar extents by both  $\gamma$ -secretase complexes, as expected. Also, the PSEN2 and PSEN1 sorting mutants did not affect significantly this cleavage, in agreement with the broad and rather uniform distribution of APP in various cellular membranes (Figures 5E to 5F'). PSEN1 and PSEN2 localization did not affect endogenous Notch ICD (NICD) production from its precursor substrate NEXT (following ectodomain shedding of mature Notch1 by ADAM family of metalloproteases), neither in conditions of naïve or delta ligand-induced Notch signaling (Figure 5G-G', S4E-E'). Thus, regulated intramembrane proteolysis of Notch1 is not confined to the cell surface. Instead, and following ectodomain shedding, NEXT is either cleaved at the cell surface or is internalized and sorted to LE/MVBs for further processing to NICD as demonstrated (Maes et al., 2014; Tagami et al., 2008). As opposed to APP, however, expression of PSEN2-S<sub>19</sub>A, which is even more depleted from the cell surface and restricted to LE/LYS and TGN, decreased NICD production, while the S<sub>19</sub>D mutation displayed more processing (Figure 5G' and S4E'). These observations suggest that Notch1 processing is affected by subtle changes in PSEN2 localization. This might be of relevance to cancer-related Notch mutations and/or the observed high variability in PSEN2 expression levels in different cancer cell lines (Figure S1A).

When we analyzed A $\beta$  production in intact cells transduced with APP-CTF (APP-C99-3xFLAG), the direct substrate of  $\gamma$ -secretase, we confirmed that PSEN2-expressing cells secrete less A $\beta$ 40 and

A $\beta$ 42 compared to PSEN1-expressing cells (Figure 5H to 5J) (Bentahir et al., 2006). Unexpectedly, this was accompanied by a significant increase in intracellular A $\beta$  (Figure 5H-I: total A $\beta$ ; Figure 5 J: A $\beta$ 40 and A $\beta$ 42). In addition, for both PSEN1- and PSEN2-expressing cells, the intracellular ratios of long to short A $\beta$  tended to be higher than those of the secreted peptides (Figure 5K), indicating that even in cells expressing WT PSENs relatively more aggregation-prone A $\beta$ 42 remains intracellularly or in the LE/LYS. Increases in intracellular A $\beta$  and decreases in secreted A $\beta$  peptides were even more pronounced with the PSEN2-S<sub>19</sub>A but not the S<sub>19</sub>D mutant, indicating that PSEN2-generated A $\beta$  in LE/LYS does not get secreted efficiently. In agreement, the AxxxAA mutant, which fails to be delivered to LE/LYS, produced low intracellular and higher extracellular amounts of A $\beta$  peptides reminiscent of PSEN1 processing (Figure 5J-J'). Similar results for total A $\beta$  were obtained in cells transduced with the APPswedish mutant (Figure S4F). Thus, our data demonstrate that the differential localization of PSEN1- and PSEN2 $\gamma$ -secretases results in differential processing of N-cadherin and Notch1, and also has important implications for the processing of APP towards intracellular A $\beta$ .

### **FAD mutations in PSEN1 and PSEN2 generate high intracellular A $\beta$ 42/40 ratios**

The >180 familial AD (FAD) mutations reported for PSEN1 are in great contrast to the limited number of FAD-PSEN2 mutations. So far, only 29 have been identified, 13 of which are pathogenic ((Canevelli et al., 2014); <http://www.molgen.vib-ua.be/ADMutations>, (Cruts et al., 2012)). No clear reason for this discrepancy currently exists. Our findings break new ground for studying the effect of FAD mutations on localization and production of intracellular A $\beta$  peptides. We introduced four FAD mutations, T122P, N141I, M239V, or M239I, into GFP-PSEN2, and expressed these constructs stably in PSEN dKO MEFs (Figure S5A). FAD mutations did not affect the subcellular localization of PSEN2, as these constructs displayed identical co-localizations with LAMP1 (Figure 6A-B) but differently affected substrate processing. Both the PSEN2 T122P and N141I mutations strongly decreased N-cadherin- and Notch-CTF processing but had no effect on AICD production (Figure 6C). The opposite effects were seen for the related FAD M239V and M239I, which mainly affected AICD production while sparing other substrates. All FAD mutations significantly decreased extracellular A $\beta$  which is caused by a major drop in A $\beta$ 40 (Figure 6D-E). While this is compensated by increased A $\beta$ 42, what was unanticipated however is

that this compensation is much more pronounced in the intracellular pool resulting in a dramatic rise in A $\beta$ 42/40 ratios, with FAD-N141I being the most extreme (A $\beta$ 42/40>50 fold compared to WT PSEN2) (Figure 6F). Hence, the FAD mutations in PSEN2 suggest that the effects on carboxypeptidase-like processing of  $\gamma$ -secretase are more strongly enhanced in the LE/LYS compartments, indicating that the localization modulates this important pathogenic aspect of PSEN function.

We next wondered whether FAD-PSEN1 mutations might affect localization and intracellular A $\beta$  generation too. We selected five common mutations and generated stably rescued dKO MEFs (Figure S5B). To our surprise, two out of five mutations (L166P and G384A) caused re-localization of GFP-PSEN1 to LAMP1-positive organelles indistinguishable from PSEN2 (Figures 6G and 6H). Similar to PSEN2, they failed to process N-cadherin-CTF to ICD while affecting other substrates to a lesser extent. Interestingly, several FAD mutations decreased NICD production while not affecting AICD or N-cadherin ICD (Figure 6I), underscoring that individual mutations differently affect major substrates which could contribute to pathology.

Again, the loss of A $\beta$ 40 concomitant with increases in A $\beta$ 42 was strongly observed in the mutations that affected the localization of PSEN1 and this most noticeably in the intracellular pool, resulting here also in the highest A $\beta$ 42/40 ratios (Figures 6K and 6L). In conclusion, we demonstrated that some FAD-PSEN1 mutations additionally act strongly on the localization of  $\gamma$ -secretase which apparently significantly promotes the generation of intracellular long A $\beta$ 42. We also obtained fibroblasts from one FAD-PSEN2 N141I patient. Remarkably, quantitative effects of total A $\beta$  were less pronounced, in line with the fact that three normal *psen* alleles are present (Fig. S5C-D). However high intracellular A $\beta$ 42 was observed, suggesting that the pathogenic allele acts as expected. In these fibroblasts we find thus a selective high intracellular A $\beta$ 42, which is not observed in control fibroblasts and independent FAD-PSEN1 patient fibroblast lines, and correlates with the more restricted LE/LYS localization of PSEN2. Importantly, the effect of such mutation is unlikely to become clear from studies limited to extracellular A $\beta$  as the main effects occur in the intracellular compartment.

## Discussion

We demonstrate here that PSEN2/ $\gamma$ -secretase is mainly restricted to a specific subcellular compartment, i.e. LE/LYS, in contrast to PSEN1/ $\gamma$ -secretase, which is broadly distributed in the cell including plasma membrane. This differential subcellular compartmentalization of the enzymes provides a mechanism for the elusive substrate specificity of the different  $\gamma$ -secretases and contradicts the dogma that  $\gamma$ -secretases indiscriminately cleave many substrates. The more restricted compartmentalization of PSEN2, in contrast to PSEN1, contributes to the intracellular pool of A $\beta$  peptide previously associated with the AD disease process (Bayer and Wirths, 2011; Gouras et al., 2010; Pensalfini et al., 2014). The fact that all FAD-PSEN2 mutations studied here most dramatically increase intracellular A $\beta$ <sub>42/40</sub> ratios, and the discovery of FAD-PSEN1 mutations that phenocopy FAD-PSEN2 mutations, put our findings also in the context of the understanding of the pathophysiology of AD, stressing the importance of the intracellular generation of aggregation-prone A $\beta$ <sub>42</sub>.

Our work focused mainly on the cellular pathways followed by the PSEN2 complex, which is targeted to LE/LYS via the selective interaction with the AP-1 adaptor complex (Figure 7). PSEN1-complexes that lack such AP-1 interaction motif follow different trafficking routes, frequenting Rab11-positive recycling endosomes, and are more abundant at the cell surface. The molecular basis for this different cell biological behavior between PSEN1 and PSEN2 is provided by a sorting signal E<sub>16</sub>RTSLM<sub>21</sub> in the PSEN2 N-terminus that had escaped attention until now. Such motif binds the  $\gamma$ 1- $\sigma$ 1 (AP1G1-AP1S1) hemicomplex of the AP-1 adaptor complex (Mattera et al., 2011) and mediates transport of PSEN2-complexes from the TGN likely via early endosomal compartments to their final residency in LE/LYS (Figures 3, 4 and 7). Mutating essential amino acids in this motif abrogates binding to AP-1, as shown by Y3H assays, pull-down experiments, and *in silico* structural analysis. This same interaction also explains the somatodendritic polarity of PSEN2 in LE/LYS compartments of primary hippocampal neurons (Figures 1G and 4C) (Bonifacino, 2014; Farias et al., 2012). Failure of PSEN2 to bind to AP-1 as evidenced by mutations in the E<sub>16</sub>RTSLM<sub>21</sub> motif results in a non-polarized distribution of PSEN2 in dendrites and axons (Figure 4C).

Two features of this motif emerge from the current study. First, the C-terminal hydrophobic Met determines specificity for AP-1 interaction. Y3H assays demonstrated that mutation of this residue to Leu confers binding to AP-2 but not AP-3, suggesting that yet other structural elements exist that prevent it

from interacting with AP-3 (Figure S2A). Second, the interaction with AP-1 is abrogated by phosphomimetic mutations of Ser<sub>19</sub> in the E<sub>16</sub>RTSLM<sub>21</sub> motif. We found that Ser<sub>19</sub> behaves as an Aurora A kinase target. Although Aurora A is predominantly known for its role in cell cycle regulation and mitosis (Nikonova et al., 2013), this kinase has recently been linked to other functions such as neurite outgrowth (Takitoh et al., 2012) and mitochondria-associated ER membrane control (Kashatus et al., 2011). Moreover, calcium release from the ER, which is affected in AD pathogenesis, might activate Aurora A (Plotnikova et al., 2010).

The Ser<sub>19</sub> to Ala mutation provides the other extreme situation. This mutant shows enhanced binding to AP-1 in co-IP experiments and displays a significant TGN localization different from the localization of wild-type PSEN2 (Figures 3G', 3G', 4D). This suggests that PSEN2 is dynamically sorted between TGN and LE/LYS and that AP-1 mediates bi-directional transport (Bonifacino, 2014). The effect of the Ser<sub>19</sub> to Ala mutation might then be explained by the enhanced interaction with AP-1, which keeps the PSEN2 mutant associated longer with exit carriers from the TGN and LE/LYS. The apparent correlation of GFP-PSEN2 S<sub>19</sub>A fluorescence with clathrin-coated tubules and vesicles in the TGN as shown by SIM-CLEM at the ultrastructural level (Figure 4G-G') supports this interpretation.

The different mutants and the transplantation experiments of the E<sub>16</sub>RTSLM<sub>21</sub> motif to PSEN1 indicate that this signal is necessary and sufficient to traffic PSEN2 to LE/LYS. Apparently the other subunits, and in particular the variable APH-1 subunit, are not required in this regulation. Other lines of evidence suggest that the APH1 subunits are responsible for the biochemical differences and/or conformations of the respective  $\gamma$ -secretases with APH-1B favoring the generation of longer A $\beta$  peptides (Acx et al., 2014; Serneels et al., 2009).

An interesting finding of our study is that localization of the PSEN2/ $\gamma$ -secretase plays a major and unanticipated role in the building up of an intracellular A $\beta$  pool. Previous work has indicated that an intraneuronal A $\beta$  progressively accumulates in AD mice models and in human AD brain (Gouras et al., 2010). Since this feature precedes the appearance of tangles and amyloid plaques, accumulation of intracellular A $\beta$  peptide might be a very early event in the pathological cascade leading to AD (Takahashi et al., 2002). We show here that PSEN2  $\gamma$ -secretase generates the main source of this intracellular pool which is instigated by its more restricted localization in LE/LYS. Interestingly intracellular accumulation of

A $\beta$  is shown to impair proper LE/MVB sorting (Almeida et al., 2006). Moreover, high local concentrations of A $\beta$  in these organelles, together with an acidic pH has profound effects on the conformation, aggregation and probably toxicity of A $\beta$  (Esbjorner et al., 2014; Hu et al., 2009) which may be further accelerated by relative increases in more toxic A $\beta$ 42 (Kuperstein et al., 2010). PSEN FAD mutations essentially affect the processivity of  $\gamma$ -secretase, resulting in release of longer A $\beta$  (Chavez-Gutierrez et al., 2012); however our work here suggests that some mutations in PSEN1 can also shift the subcellular localization to LE/LYS which is directly correlated with increased intracellular A $\beta$ 42 at the expense of A $\beta$ 40 much alike mutations in PSEN2. This adds an important and completely unexpected cellular dimension that potentially could impact our understanding of the pathological effects of FAD-PSEN and in particular FAD-PSEN2 mutations. Given the strikingly congruent effects of all PSEN2 mutations studied here, we speculate that intracellular A $\beta$  toxicity may lead to LE/LYS dysfunction causing a profound disturbance of proteostasis in the affected cells. It is too early to speculate that this mechanisms could ultimately also play in other forms of AD. At least several FAD-PSEN1 mutations caused re-localization to LE/LYS thereby mimicking the FAD-PSEN2 effects, also with respect to substrate processing. It is possible that in other mutations the effects on production of A $\beta$  dominate the picture, but even there it is possible that long A $\beta$  gets endocytosed and accumulates in the intracellular compartment.

Furthermore, it should be realized that almost all FAD-PSEN1 mutations studied so far result in enzymes that are relatively less efficient in processing than their wild-type counterparts (Chavez-Gutierrez et al., 2012). This may cause spillover of APP-CTF to the PSEN2 complex, resulting in the production of more A $\beta$  in acidic compartments, where A $\beta$  is more prone to aggregation (Esbjorner et al., 2014; Hu et al., 2009). Secondly, it should be noted that early disturbances in endo/lysosomal compartments have been documented as an early characteristic of AD brain ((Cataldo et al., 2000; Ginsberg et al., 2010), reviewed in (Peric and Annaert, 2015)) and GWAS studies have also evidenced the crucial role of the endolysosomal sorting system in sporadic AD (Karch and Goate, 2015). Our work may indeed provide an important clue towards the understanding of a crucial pathogenic circle in AD: abnormal processing of APP-CTF (as occurs in FAD) in endo/lysosomes might affect their function; reversibly subtle alterations in trafficking of APP or in endo/lysosomal biology might deviate A $\beta$



generation to these compartments, increasing the pool of intracellular A $\beta$  and causing AD in a pernicious feed-forward cycle.

The physiologically most important conclusion from the current work is that sub-compartmentalization of the different  $\gamma$ -secretases and their substrates provides specificity as well as spatial and temporal control of their proteolytic activities. Instead of being specific “proteasomes of the membrane” (Kopan and Ilagan, 2004),  $\gamma$ -secretases appear to function as intriguingly spatially regulated enzymes with precise functions in different physiological pathways. Additional work in proper cellular and mouse models is needed to further support the potential importance for AD pathogenesis and which may provide a rationale for the development of PSEN2/ $\gamma$ -secretase specific inhibitors that will act at the heart of intracellular A $\beta$  generation.

## Experimental procedures

Additional procedures and details are in Supplemental Experimental Procedures.

### SIM-CLEM

GFP-PSEN2 rescued cells grown on glass bottom dishes co-expressing LAMP1-mCherry or labeled with MitoTracker were fixed and Z-sections generated by SIM followed by EM processing.

### Molecular Modeling

The structure of the AP1 core (PDBID: 4P6Z) was used as template for modelling binding with the PSEN2 peptide motif VCDERTSLMS using FoldX force field (Schymkowitz et al., 2005). Effects of mutations on interaction energies was analyzed using BuildModel and Analyze Complex command. Molecular graphics were generated with YASARA (Krieger et al., 2002).

### PSEN1 and PSEN2 knockout MNT-1 cells

CRISPR Design Tool (<http://www.genome-engineering.org/crispr/>) was used to select the genomic sequence target in *hPSEN1* (5'-ggatggactgcgtggctcat-3') and *hPSEN2* (5'-gaccgctatgtctgtagtgg3'). Oligo pairs encoding 20 nucleotides guide sequences were annealed and ligated into the plasmid pX330 (Addgene). MNT-1 cells were transfected using JetPRIME and KO clones selected by serial dilution.

### Isolation of LE/LYS

Cells were incubated (15 min, 37°C) with DMSA-coated SPIONs (0.2 mg/ml), washed with PBS, and incubated in fresh medium (4 h, 37°C). Harvested cells were centrifuged (180g, 10 min) and pellets resuspended in homogenization buffer (HB; 250 mM sucrose, 5 mM Tris and 1 mM EGTA pH 7.4 supplemented with PI). After cell cracking a postnuclear supernatant was loaded on a LS column placed in a strong magnetic field (0.5 T, SuperMACSII, Miltenyi). Nonmagnetic material was removed and after detachment from the magnet, the bound LE/LYS were eluted, centrifuged (126,000g, 1 h) and analyzed.

### A $\beta$

Cells were processed 24 h after transfection with C99-3xFLAG (or APP<sup>sw</sup>). Conditioned media were cleared by centrifugation and cells lysed in lysis buffer (50 mM Tris-HCL, pH 7.4; 150 mM NaCl; 1% Triton X-100; 0.1% SDS; 0.5% sodium deoxycholate). Total A $\beta$  was detected by Western blot (6E10 antibody). A $\beta$ 40 and -42 were quantified by ELISA (JRF/cAb40/28 antibody for A $\beta$ 1-40, JRF/cAb42/26 for A $\beta$ 1-42, and detection antibody JRF/AbN/25).

**Supplemental information** includes Supplemental Experimental procedures, five figures, and two movies.

## **Author Contributions**

RS and WA designed experiments. RS, CE, VB, WV and CM generated PSEN hybrids, dKO rescue lines and MNT-1 KO, and performed biochemical assays. PE analyzed FAD-PSEN lines. LR and GvN did melanosome-related EM. AKT, RW and KD did organelle isolations. RH, AG and MV provided Notch data and VDW, MB, RD and EW phosphorylation data. Confocal analysis was done by RS and SM. KV, PE and PB optimized SIM-CLEM. GDB, JS and FR did in silico analysis. RM and JSB contributed with Y3H. MM and BDS provided A $\beta$  ELISA. WA and RS wrote the manuscript with input from all authors.

## **Acknowledgements**

Financial support was from VIB (WA, BDS, FR, JS), KU Leuven (C16/15/073 and IDO/12/020 to WA), federal government (IAP P7/16: WA, BDS, FR, JS), Hercules (AKUL/09/037, 11/30, 13/39 to WA), SAO (S#14017 to WA) and NICHD Intramural Program (ZIA HD001607 to JSB). AKT and GDB held PhD fellowships of VIB and IWT. We thank K. Ivanova for initial FP-PSEN rescue. PE was a Marie-Curie postdoc. AG, RH and MV are supported by EU-ERC (208259); LR and GvN by “Fondation ARC” (n°DOC20130606986 and # PJA20131200286). We thank PICT-IBiSA (Institut Curie, Paris) and France-BioImaging (ANR-10-INSB-04).

## References

- Acx, H., Chavez-Gutierrez, L., Serneels, L., Lismont, S., Benurwar, M., Elad, N., and De Strooper, B. (2014). Signature amyloid beta profiles are produced by different gamma-secretase complexes. *The Journal of biological chemistry* 289, 4346-4355.
- Almeida, C.G., Takahashi, R.H., and Gouras, G.K. (2006). Beta-amyloid accumulation impairs multivesicular body sorting by inhibiting the ubiquitin-proteasome system. *The Journal of neuroscience : the official journal of the Society for Neuroscience* 26, 4277-4288.
- Bayer, T.A., and Wirths, O. (2011). Intraneuronal Abeta as a trigger for neuron loss: can this be translated into human pathology? *Biochemical Society transactions* 39, 857-861.
- Bentahir, M., Nyabi, O., Verhamme, J., Tolia, A., Horre, K., Wiltfang, J., Esselmann, H., and De Strooper, B. (2006). Presenilin clinical mutations can affect gamma-secretase activity by different mechanisms. *Journal of neurochemistry* 96, 732-742.
- Bonifacino, J.S. (2014). Adaptor proteins involved in polarized sorting. *The Journal of cell biology* 204, 7-17.
- Braulke, T., and Bonifacino, J.S. (2009). Sorting of lysosomal proteins. *Biochimica et biophysica acta* 1793, 605-614.
- Canevelli, M., Piscopo, P., Talarico, G., Vanacore, N., Blasimme, A., Crestini, A., Tosto, G., Troili, F., Lenzi, G.L., Confaloni, A., *et al.* (2014). Familial Alzheimer's disease sustained by presenilin 2 mutations: systematic review of literature and genotype-phenotype correlation. *Neuroscience and biobehavioral reviews* 42, 170-179.
- Cataldo, A.M., Peterhoff, C.M., Troncoso, J.C., Gomez-Isla, T., Hyman, B.T., and Nixon, R.A. (2000). Endocytic pathway abnormalities precede amyloid beta deposition in sporadic Alzheimer's disease and Down syndrome: differential effects of APOE genotype and presenilin mutations. *The American journal of pathology* 157, 277-286.
- Chavez-Gutierrez, L., Bammens, L., Benilova, I., Vandersteen, A., Benurwar, M., Borgers, M., Lismont, S., Zhou, L., Van Cleynenbreugel, S., Esselmann, H., *et al.* (2012). The mechanism of gamma-Secretase dysfunction in familial Alzheimer disease. *The EMBO journal* 31, 2261-2274.
- Cruts, M., Theuns, J., and Van Broeckhoven, C. (2012). Locus-specific mutation databases for neurodegenerative brain diseases. *Human mutation* 33, 1340-1344.
- De Strooper, B., and Annaert, W. (2010). Novel research horizons for presenilins and gamma-secretases in cell biology and disease. *Annual review of cell and developmental biology* 26, 235-260.
- Edbauer, D., Winkler, E., Regula, J.T., Pesold, B., Steiner, H., and Haass, C. (2003). Reconstitution of gamma-secretase activity. *Nature cell biology* 5, 486-488.
- Esbjorner, E.K., Chan, F., Rees, E., Erdelyi, M., Luheshi, L.M., Bertoncini, C.W., Kaminski, C.F., Dobson, C.M., and Kaminski Schierle, G.S. (2014). Direct observations of amyloid beta self-assembly in live cells provide insights into differences in the kinetics of Abeta(1-40) and Abeta(1-42) aggregation. *Chemistry & biology* 21, 732-742.
- Farias, G.G., Cuitino, L., Guo, X., Ren, X., Jarnik, M., Mattera, R., and Bonifacino, J.S. (2012). Signal-mediated, AP-1/clathrin-dependent sorting of transmembrane receptors to the somatodendritic domain of hippocampal neurons. *Neuron* 75, 810-823.
- Freeman, M. (2014). The Rhomboid-Like Superfamily: Molecular Mechanisms and Biological Roles. *Annual review of cell and developmental biology*.
- Friedrich, R.P., Tepper, K., Ronicke, R., Soom, M., Westermann, M., Reymann, K., Kaether, C., and Fandrich, M. (2010). Mechanism of amyloid plaque formation suggests an intracellular basis of Abeta pathogenicity. *Proceedings of the National Academy of Sciences of the United States of America* 107, 1942-1947.

Ginsberg, S.D., Alldred, M.J., Counts, S.E., Cataldo, A.M., Neve, R.L., Jiang, Y., Wu, J., Chao, M.V., Mufson, E.J., Nixon, R.A., *et al.* (2010). Microarray analysis of hippocampal CA1 neurons implicates early endosomal dysfunction during Alzheimer's disease progression. *Biological psychiatry* 68, 885-893.

Golde, T.E., Wolfe, M.S., and Greenbaum, D.C. (2009). Signal peptide peptidases: a family of intramembrane-cleaving proteases that cleave type 2 transmembrane proteins. *Seminars in cell & developmental biology* 20, 225-230.

Gouras, G.K., Tampellini, D., Takahashi, R.H., and Capetillo-Zarate, E. (2010). Intraneuronal beta-amyloid accumulation and synapse pathology in Alzheimer's disease. *Acta neuropathologica* 119, 523-541.

Hu, X., Crick, S.L., Bu, G., Frieden, C., Pappu, R.V., and Lee, J.M. (2009). Amyloid seeds formed by cellular uptake, concentration, and aggregation of the amyloid-beta peptide. *Proceedings of the National Academy of Sciences of the United States of America* 106, 20324-20329.

Jia, X., Weber, E., Tokarev, A., Lewinski, M., Rizk, M., Suarez, M., Guatelli, J., and Xiong, Y. (2014). Structural basis of HIV-1 Vpu-mediated BST2 antagonism via hijacking of the clathrin adaptor protein complex 1. *eLife* 3, e02362.

Jurisch-Yaksi, N., Sannerud, R., and Annaert, W. (2013). A fast growing spectrum of biological functions of gamma-secretase in development and disease. *Biochimica et biophysica acta* 1828, 2815-2827.

Karch, C.M., and Goate, A.M. (2015). Alzheimer's disease risk genes and mechanisms of disease pathogenesis. *Biological psychiatry* 77, 43-51.

Kashatus, D.F., Lim, K.H., Brady, D.C., Pershing, N.L., Cox, A.D., and Counter, C.M. (2011). RALA and RALBP1 regulate mitochondrial fission at mitosis. *Nature cell biology* 13, 1108-1115.

Kelly, B.T., McCoy, A.J., Spate, K., Miller, S.E., Evans, P.R., Honing, S., and Owen, D.J. (2008). A structural explanation for the binding of endocytic dileucine motifs by the AP2 complex. *Nature* 456, 976-979.

Kopan, R., and Ilagan, M.X. (2004). Gamma-secretase: proteasome of the membrane? *Nature reviews Molecular cell biology* 5, 499-504.

Krawitz, P., Haffner, C., Fluhrer, R., Steiner, H., Schmid, B., and Haass, C. (2005). Differential localization and identification of a critical aspartate suggest non-redundant proteolytic functions of the presenilin homologues SPPL2b and SPPL3. *The Journal of biological chemistry* 280, 39515-39523.

Krieger, E., Koraimann, G., and Vriend, G. (2002). Increasing the precision of comparative models with YASARA NOVA--a self-parameterizing force field. *Proteins* 47, 393-402.

Kuperstein, I., Broersen, K., Benilova, I., Rozenski, J., Jonckheere, W., Debulpaep, M., Vandersteen, A., Segers-Nolten, I., Van Der Werf, K., Subramaniam, V., *et al.* (2010). Neurotoxicity of Alzheimer's disease Abeta peptides is induced by small changes in the Abeta42 to Abeta40 ratio. *The EMBO journal* 29, 3408-3420.

Maes, H., Kuchnio, A., Peric, A., Moens, S., Nys, K., De Bock, K., Quaegebeur, A., Schoors, S., Georgiadou, M., Wouters, J., *et al.* (2014). Tumor vessel normalization by chloroquine independent of autophagy. *Cancer cell* 26, 190-206.

Mattera, R., Boehm, M., Chaudhuri, R., Prabhu, Y., and Bonifacino, J.S. (2011). Conservation and diversification of dileucine signal recognition by adaptor protein (AP) complex variants. *The Journal of biological chemistry* 286, 2022-2030.

Nikonova, A.S., Astsaturov, I., Serebriiskii, I.G., Dunbrack, R.L., Jr., and Golemis, E.A. (2013). Aurora A kinase (AURKA) in normal and pathological cell division. *Cellular and molecular life sciences : CMLS* 70, 661-687.

- Peden, A.A., Oorschot, V., Hesser, B.A., Austin, C.D., Scheller, R.H., and Klumperman, J. (2004). Localization of the AP-3 adaptor complex defines a novel endosomal exit site for lysosomal membrane proteins. *The Journal of cell biology* 164, 1065-1076.
- Pensalfini, A., Albay, R., 3rd, Rasool, S., Wu, J.W., Hatami, A., Arai, H., Margol, L., Milton, S., Poon, W.W., Corrada, M.M., *et al.* (2014). Intracellular amyloid and the neuronal origin of Alzheimer neuritic plaques. *Neurobiology of disease* 71, 53-61.
- Perez, R.G., Soriano, S., Hayes, J.D., Ostaszewski, B., Xia, W., Selkoe, D.J., Chen, X., Stokin, G.B., and Koo, E.H. (1999). Mutagenesis identifies new signals for beta-amyloid precursor protein endocytosis, turnover, and the generation of secreted fragments, including Abeta42. *The Journal of biological chemistry* 274, 18851-18856.
- Peric, A., and Annaert, W. (2015). Early etiology of Alzheimer's disease: tipping the balance toward autophagy or endosomal dysfunction? *Acta neuropathologica* 129, 363-381.
- Plotnikova, O.V., Pugacheva, E.N., Dunbrack, R.L., and Golemis, E.A. (2010). Rapid calcium-dependent activation of Aurora-A kinase. *Nature communications* 1, 64.
- Raposo, G., and Marks, M.S. (2007). Melanosomes--dark organelles enlighten endosomal membrane transport. *Nature reviews Molecular cell biology* 8, 786-797.
- Saftig, P., and Klumperman, J. (2009). Lysosome biogenesis and lysosomal membrane proteins: trafficking meets function. *Nature reviews Molecular cell biology* 10, 623-635.
- Sannerud, R., and Annaert, W. (2009). Trafficking, a key player in regulated intramembrane proteolysis. *Seminars in cell & developmental biology* 20, 183-190.
- Schymkowitz, J., Borg, J., Stricher, F., Nys, R., Rousseau, F., and Serrano, L. (2005). The FoldX web server: an online force field. *Nucleic acids research* 33, W382-388.
- Serneels, L., Dejaegere, T., Craessaerts, K., Horre, K., Jorissen, E., Tousseyn, T., Hebert, S., Coolen, M., Martens, G., Zwijsen, A., *et al.* (2005). Differential contribution of the three Aph1 genes to gamma-secretase activity in vivo. *Proceedings of the National Academy of Sciences of the United States of America* 102, 1719-1724.
- Serneels, L., Van Biervliet, J., Craessaerts, K., Dejaegere, T., Horre, K., Van Houtvin, T., Esselmann, H., Paul, S., Schafer, M.K., Berezovska, O., *et al.* (2009). gamma-Secretase heterogeneity in the Aph1 subunit: relevance for Alzheimer's disease. *Science* 324, 639-642.
- Tagami, S., Okochi, M., Yanagida, K., Ikuta, A., Fukumori, A., Matsumoto, N., Ishizuka-Katsura, Y., Nakayama, T., Itoh, N., Jiang, J., *et al.* (2008). Regulation of Notch signaling by dynamic changes in the precision of S3 cleavage of Notch-1. *Molecular and cellular biology* 28, 165-176.
- Takahashi, R.H., Nam, E.E., Edgar, M., and Gouras, G.K. (2002). Alzheimer beta-amyloid peptides: normal and abnormal localization. *Histology and histopathology* 17, 239-246.
- Takasugi, N., Tomita, T., Hayashi, I., Tsuruoka, M., Niimura, M., Takahashi, Y., Thinakaran, G., and Iwatsubo, T. (2003). The role of presenilin cofactors in the gamma-secretase complex. *Nature* 422, 438-441.
- Takitoh, T., Kumamoto, K., Wang, C.C., Sato, M., Toba, S., Wynshaw-Boris, A., and Hirotsune, S. (2012). Activation of Aurora-A is essential for neuronal migration via modulation of microtubule organization. *The Journal of neuroscience : the official journal of the Society for Neuroscience* 32, 11050-11066.
- Traub, L.M., and Bonifacino, J.S. (2013). Cargo recognition in clathrin-mediated endocytosis. *Cold Spring Harbor perspectives in biology* 5, a016790.
- Voss, M., Schroder, B., and Fluhrer, R. (2013). Mechanism, specificity, and physiology of signal peptide peptidase (SPP) and SPP-like proteases. *Biochimica et biophysica acta* 1828, 2828-2839.
- Walter, J., Capell, A., Grunberg, J., Pesold, B., Schindzielorz, A., Prior, R., Podlisny, M.B., Fraser, P., Hyslop, P.S., Selkoe, D.J., *et al.* (1996). The Alzheimer's disease-associated

presenilins are differentially phosphorylated proteins located predominantly within the endoplasmic reticulum. *Mol Med* 2, 673-691.

Wang, R., Tang, P., Wang, P., Boissy, R.E., and Zheng, H. (2006). Regulation of tyrosinase trafficking and processing by presenilins: partial loss of function by familial Alzheimer's disease mutation. *Proceedings of the National Academy of Sciences of the United States of America* 103, 353-358.

Watt, B., van Niel, G., Raposo, G., and Marks, M.S. (2013). PMEL: a pigment cell-specific model for functional amyloid formation. *Pigment cell & melanoma research* 26, 300-315.

Wolfe, M.S. (2009). Intramembrane-cleaving proteases. *The Journal of biological chemistry* 284, 13969-13973.



## Figure legends

### Figure 1: PSEN1 and PSEN2 have distinct subcellular distributions.

(A) Discontinuous sucrose/D<sub>2</sub>O flotation gradient of WT MEF postnuclear supernatant analyzed by Western blot using compartment specific antibodies. De novo A $\beta$  production measured using a cell free assay.

(A') Quantification of the enrichments from (A) for PSEN1 (blue), PSEN2 (orange) and  $\gamma$ -secretase activity (A $\beta$ , red, mean  $\pm$  SEM, n=2 for PSENs, n=4 for A $\beta$ ).

(B-C) Quantitative Western blot of LE/LYS isolated using SPIONs (B) and cell surface biotinylated PSENs and nicastrin (NCT). (B-C') (mean  $\pm$  SEM, n=3).

(D-E) as in (B-C) for the indicated cell lines (mean  $\pm$ SEM, n=2-4

(F) Double immunostaining of endogenous PSEN2 and LAMP1 confirming LE/LYS enrichment for PSEN2 in indicated cell lines. Bar= 10  $\mu$ m.

(G-H) Endogenous PSEN2 co-localizes with LAMP1 in murine primary hippocampal neurons (DIV 7, G) and in brain cerebral cortex area (P10, H). Inset in G: zoomed area. Bar= 10  $\mu$ m. (H) Merge 2 (subicular area) and 3: respective zoomed area of the square in merge 1 and 2. Merge 1: Bar= 200  $\mu$ m, merge 2, 3: Bar= 10  $\mu$ m.

(I) Western blot analysis of PSEN dKO MEFs and dKO MEFs stably rescued with GFP-PSEN1 or GFP-PSEN2 demonstrates restored  $\gamma$ -secretase assembly and activity.

(J-J') Quantitative Western blot of cell surface biotinylated GFP-PSEN1 and -PSEN2 shows more GFP-PSEN1 at the cell surface (mean  $\pm$  SEM, n=4).

(K) Co-localization of GFP-PSEN1 (top) and GFP-PSEN2 (bottom) with endogenous LAMP1. Insets and right panel: zoomed areas. Bar=10  $\mu$ m.

(L) Primary hippocampal neurons (DIV7) expressing GFP-PSEN1 (green, top), or GFP-PSEN2 (green, bottom) labeled with LysoTracker red (50 nM). Inset: GFP-PSEN2 co-localizes with LysoTracker. Bar=10  $\mu$ m.

See also Figure S1.

### Figure 2: Cytosolic N-terminus of PSEN2 is responsible for its localization to LE/LYS.

(A) Scheme of GFP-PSEN1 (blue) and GFP-PSEN2 (orange) WT and hybrids (1 to 5, see supplemental info), with nine transmembrane domains (white squares) and endoproteolytic cleavage site (dotted line).

(B) Western blot of dKO MEFs rescued with GFP-PSEN hybrids. All hybrids rescue  $\gamma$ -secretase assembly and activity.

(C) Co-localization of GFP-PSEN hybrids with endogenous LAMP1. Right: zoomed area. Bar= 10  $\mu$ m.

(C') Quantification of (C) using Manders' coefficient (mean  $\pm$  SEM, n=3,  $\geq$ 30 cells per experiment).

### Figure 3: Adaptor complex AP-1 binds the N-terminal conserved E<sub>16</sub>RTSLM<sub>21</sub> motif in PSEN2.

(A) Alignment of human PSEN1 and PSEN2 N-termini (top). PSEN2 N-terminus includes an acidic cluster with a conserved ERTSLM sequence (red box and lower panel) resembling the consensus [D/E]XXXL[L/I/M] and three conserved phosphorylatable serines (red). Scheme shows point mutations used in this study.

(B) T-vectors used in Y3H.

(C) Y3H shows that PSEN2 tail interacts with AP-1  $\gamma$ 1- $\sigma$ 1A but not with AP-2  $\alpha$ C- $\sigma$ 2 or AP-3  $\delta$ - $\sigma$ 3A. This interaction is impaired by combined replacement of Glu16, Leu20 and Met21 for Ala (PSEN2-AxxxAA). Note selective interaction of the control Nef dileucine signal with AP-1  $\gamma$ 1- $\sigma$ 1A, AP-2  $\alpha$ C- $\sigma$ 2 and AP-3  $\delta$ - $\sigma$ 3A and not with mismatched combinations of AP subunits.

(D) PSEN2 tail-AP-1  $\gamma$ 1- $\sigma$ 1A interaction is impaired by individual Ala substitution in the PSEN2 motif. While the S<sub>19</sub>A substitution is inconsequential, the phosphorylation-mimicking S<sub>19</sub>D substitution abolishes interaction.

(E) Western blot analysis of pull-downs of rat brain extracts with recombinant GST, GST-N<sub>1-81</sub>PSEN1 and GST-N<sub>1-86</sub>PSEN2.

(F) Same as in (E) but for single or triple Ala substitutions in the ERTSLM motif (top) and Ser to Ala/Asp mutations in N-terminus (bottom) of GST-N<sub>1-86</sub>PSEN2. Coomassie staining shows equal loading of GST-fusion proteins.

(G-G') Co-immunoprecipitation of CHAPSO-extracts from dKO MEFs (control) and rescued cells using anti-GFP antibody. Western blot (G, quantified in G') with anti-AP-1- $\gamma$ 1 shows increased binding to GFP-PSEN2-S<sub>19</sub>A compared to PSEN2 WT (mean  $\pm$  SEM n=3, \*\*\*  $p$ <0.001, \* $p$ <0.05).

(H) Surface representation of the  $\sigma$ 1 subunit (blue) and  $\gamma$ 1 subunit (green) of AP-1 hemicomplex with the VCDERTSLMS peptide from PSEN2 (gray) in the binding groove of the  $\sigma$ 1 subunit. Glu (red) and Leu/Met (purple) interact with the  $\gamma$ 1 and  $\sigma$ 1 subunit, respectively. The phospho group on Ser<sub>19</sub> which disfavors interaction, is marked in yellow/red.

(I) Theoretical effect of mutations on the interaction energy between the 'CDERTSLMS' motif and the AP-1 hemicomplex calculated using FoldX forcefield. All mutations, except S<sub>19</sub>A, strongly destabilize interaction (high (>1) positive  $\Delta\Delta G$  (kcal.mol<sup>-1</sup>)).

(J) *In vitro* kinase assays using purified GST-PSEN2 WT and mutants as substrates incubated with CKII, CKI or Aurora A. Top: autoradiograph of phosphorylated GST fusion proteins. Note very low labeling of fusion proteins by CK1 compared to control (Casein). Middle: colloidal staining shows equal loading. Bottom: quantification of <sup>32</sup>P incorporation in GST-fusion proteins as a ratio to colloidal gold staining (mean  $\pm$  SEM n=3, \*\*\*  $p$ <0.001)

See also Figures S2.

**Figure 4: E<sub>16</sub>RTSLM<sub>21</sub> motif in PSEN2 is sufficient for its LE/LYS localization.**

(A) Double immunostaining shows strong overlap of GFP-PSEN2-S19A but not -AxxxAA with LAMP1. Right: zoomed area. Bar=10  $\mu$ m. (A') Quantification using Mander's coefficient (mean  $\pm$  SEM, n=3,  $\geq$ 30 cells per experiment).

(B-B') Quantitative Western blot of cell surface biotinylated NCT and PSEN2-CTF for GFP-PSEN2 WT and mutant rescued cells shows low amount of S<sub>19</sub>A at the cell surface (mean ± SEM, n=4, \**p*<0.05, \*\*\**p*<0.001).

(C) Triple fluorescent labeling of primary hippocampal neurons (DIV7) shows PSEN1 localization in axons (tau1) and dendrites (MAP2) while PSEN2 (but not PSEN2-AxxxAA) is solely present in dendrites. Bar=10µm. (C') Polarity index (axonal/dendritic signal) calculated for GFP-PSEN1 (n=28), GFP-PSEN2 (n=31) and GFP-PSEN-AxxxAA (n=22) (mean ± SEM, \*\*\**p*<0.001).

(D) Partial co-localization of GFP-PSEN2-S<sub>19</sub>A with TGN46. Right: Zoomed area. Bar=10 µm.

(E) GFP-PSEN2-S<sub>19</sub>A co-localizes with endogenous AP-1 (AP1G1) at the TGN and on emanating tubular structures (inset). Bar= 5 µm.

SIM image of GFP-PSEN2-WT (F) and -S<sub>19</sub>A cells (G) co-transfected with LAMP1-mCherry: area indicated by a square is analyzed by CLEM (F' and G'). G: Golgi; Mit: mitochondria; arrowheads: clathrin coated vesicles; empty arrowhead: endosome with flat clathrin-coated domain; arrows: tubular structures. (F, G) Bar= 10µm (F,G) and 1µm (F', G').

See also Figure S3, Movies S1 and S2.

### **Figure 5: Subcellular localization of γ-secretase regulates substrate accessibility.**

(A-A') Quantitative Western blot of siRNA-treated MNT-1 cells (mean ± SEM, n=3).

(B) Transmission EM of WT and PSEN2-siRNA treated MNT-1 cells. I to IV indicate different stages of melanosome maturation. PSEN2 knockdown results in more immature stages. Arrows in insets specify stage II melanosomes containing normal and very thin fibrils in WT (Ctrl), and PSEN2 knockdown cells, respectively. Bar=1µm.

(C) Western blot analysis of WT MNT-1 (Ctrl) and single PSEN2 (two clones) and PSEN1 (one clone) KO cells generated using CRISPR/Cas9.

(D) Transmission EM of WT (Ctrl) and PSEN2-KO (clone 18) MNT-1 cells. Insets: round shaped unstructured immature melanosomes (arrows) accumulate in PSEN2-KO cells at the expense of mature stage II, III and IV melanosomes. Bar=500nm.

(D') Quantification of (D) as percentage of each compartment relative to total compartments.

(E-G) Western blot demonstrating ICD production from endogenous N-cadherin-, APP- and Notch1-CTFs from membrane fractions of dKO MEFs rescued with GFP-PSEN1 or -PSEN2 as indicated. (E'-G') Quantification of (E-G) (mean ± SEM, n=4-5).

(H-I) Western blot of intracellular and secreted Aβ from total lysate (bottom) and conditioned media (top) (quantified in I).

(J-K) ELISA of intracellular and extracellular Aβ40 and 42, including Aβ42/40 (mean ± SEM, n=7). For all graphs: \**p*<0.05, \**p*<0.01, \*\*\**p*<0.001

See also Figure S4.

### **Figure 6: Most intracellular A $\beta$ is generated by PSEN2 $\gamma$ -secretase.**

(A-B) FAD mutations do not affect co-localization of PSEN2 with LAMP1 in LE/LYS. Bottom: zoomed area. Bar=10  $\mu$ m. (B) Overlap quantified using Mander's coefficient (mean  $\pm$  SEM, n=3,  $\geq$ 30 cells per experiment).

(C) Quantification of ICD production from indicated substrates starting from membrane fractions of PSEN2 WT or PSEN2-FAD rescued cell lines (mean  $\pm$  SEM; n=5).

(D) Quantitative Western blot of total secreted and intracellular A $\beta$  from PSEN2-WT and -FAD rescued cells (mean  $\pm$  SEM; n=6).

(E) as in (D) but using ELISA to quantify secreted and intracellular A $\beta$ 40 and -42 as well as A $\beta$ 42/40 ratios (F) (mean  $\pm$  SEM; n=6).

(G-H) as in (A-B) but for GFP-PSEN1 WT and FAD mutants.

(I) as in (C): Note that FAD PSEN1-L166P and G384A are unable to process N-cadherin CTF.

(J-L) as in (D-F). PSEN1 mutations most strongly increase intracellular 42/40 ratio with highest ratio for L166P and G384A.

(C, D, E, I, J, K) \* $p$ <0.05; \*\* $p$ <0.01; \*\*\* $p$ <0.001.

See also Figures S5.

### **Figure 7: Distinct endosomal transport itineraries of PSEN1 and PSEN2.**

PSEN1 (yellow) complexes are sorted from the TGN to the cell surface likely via the Rab11-positive recycling compartments. In contrast, interaction with AP-1 via a conserved ERTSLM-motif allows PSEN2 (red) complexes to be sorted to LE/LYS, probable via early/sorting endosomes. Phosphorylation of Ser<sub>19</sub> affects PSEN2 sorting. Mutation to Ala confers a more strict localization in LE/LYS and TGN.

Substituting Ser<sub>19</sub> to Asp (phosphomimetic) decreases binding and results in a more randomized distribution. Changing critical residues in the motif (AxxxAA) fully prevents AP-1 binding, resulting in "default" sorting of PSEN2/ $\gamma$ -secretase along the PSEN1/ $\gamma$ -secretase transport route (red dashed arrow). LE/LYS Localization of PSEN2/ $\gamma$ -secretase accounts for a major pool of intracellular A $\beta$ , wherein relative A $\beta$ 42 levels become strongly increased by FAD mutations.

# FIGURE 1

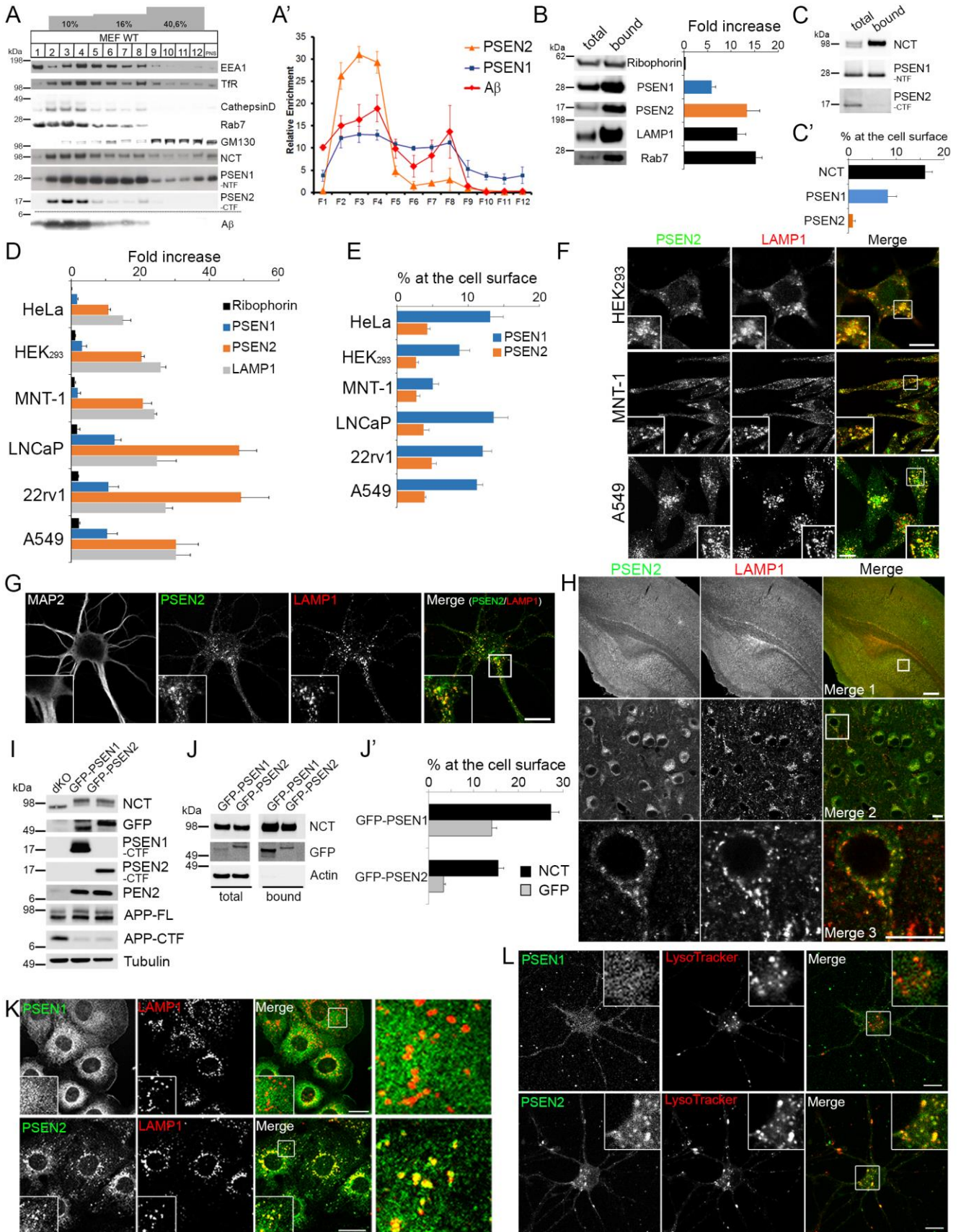


## FIGURE 2

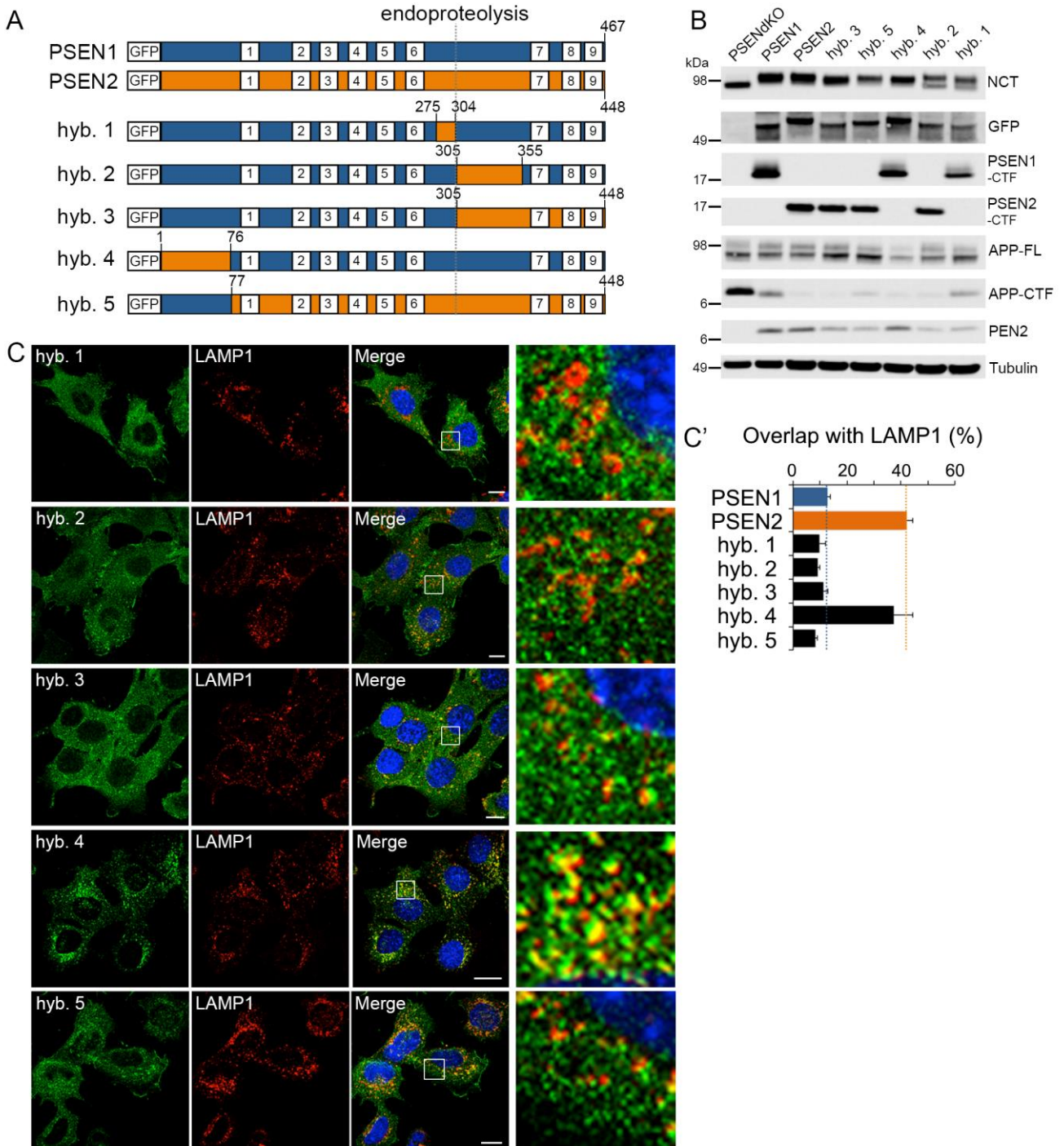


# FIGURE 3

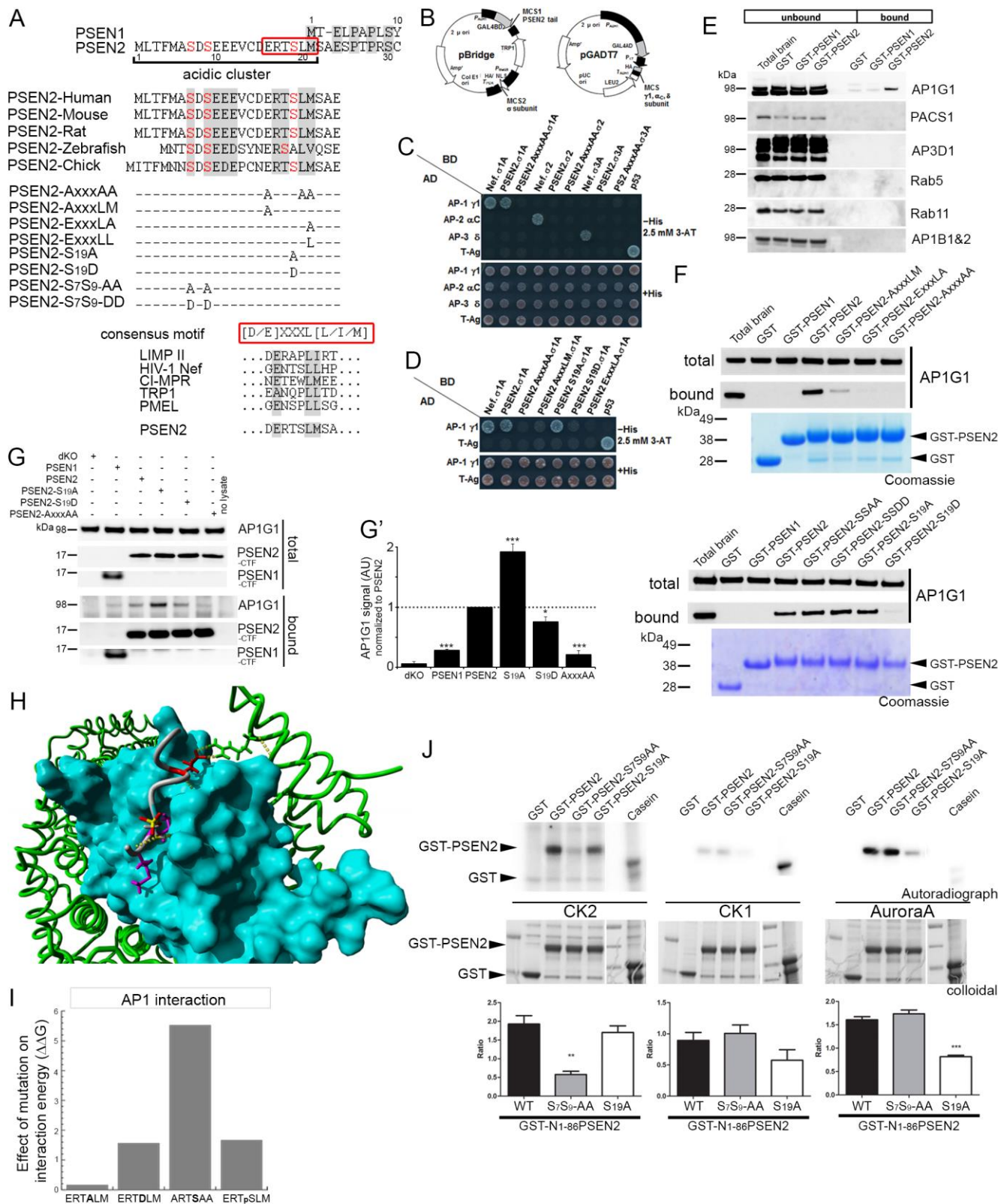


**FIGURE 4**

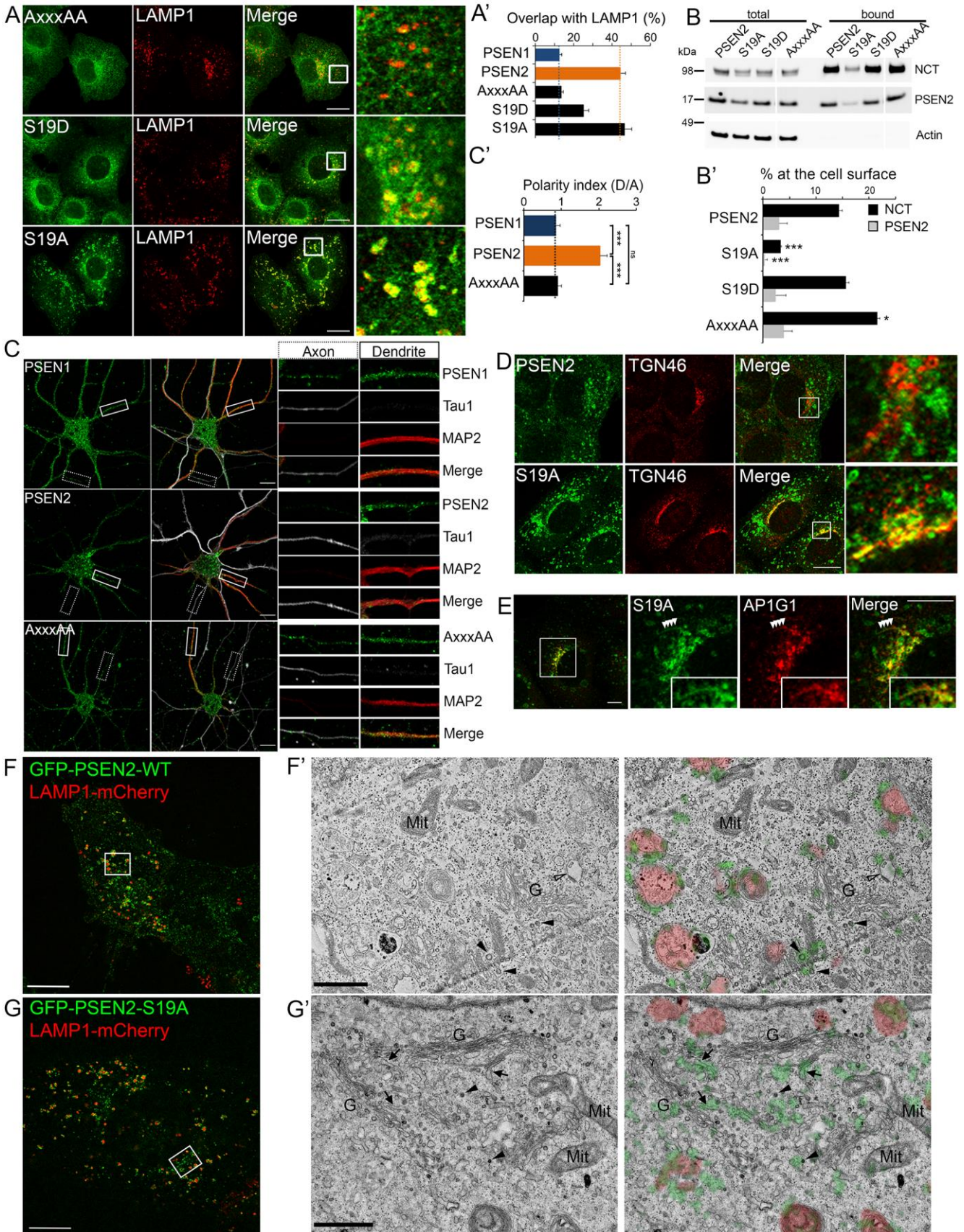




# FIGURE 5

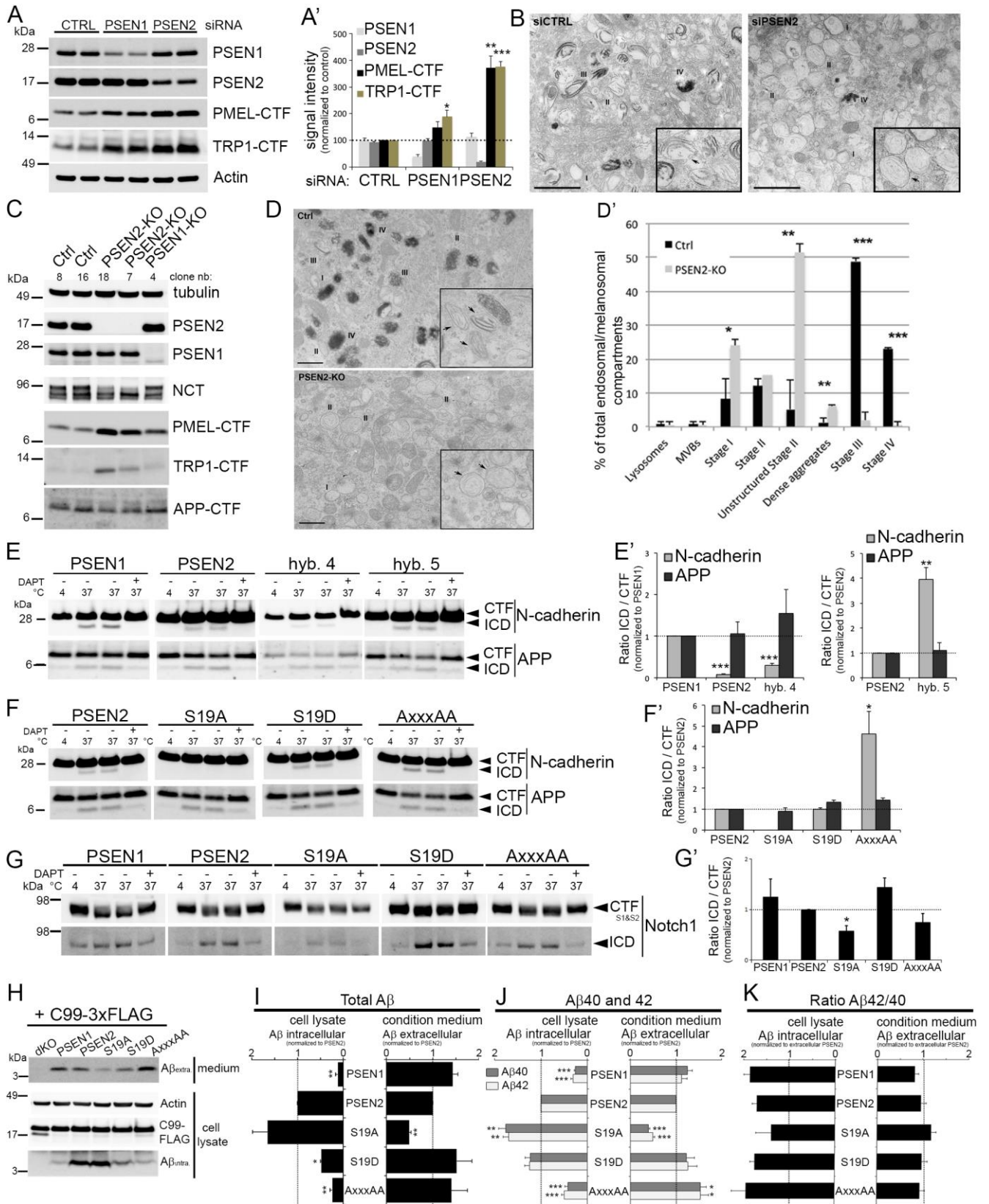


**FIGURE 6**

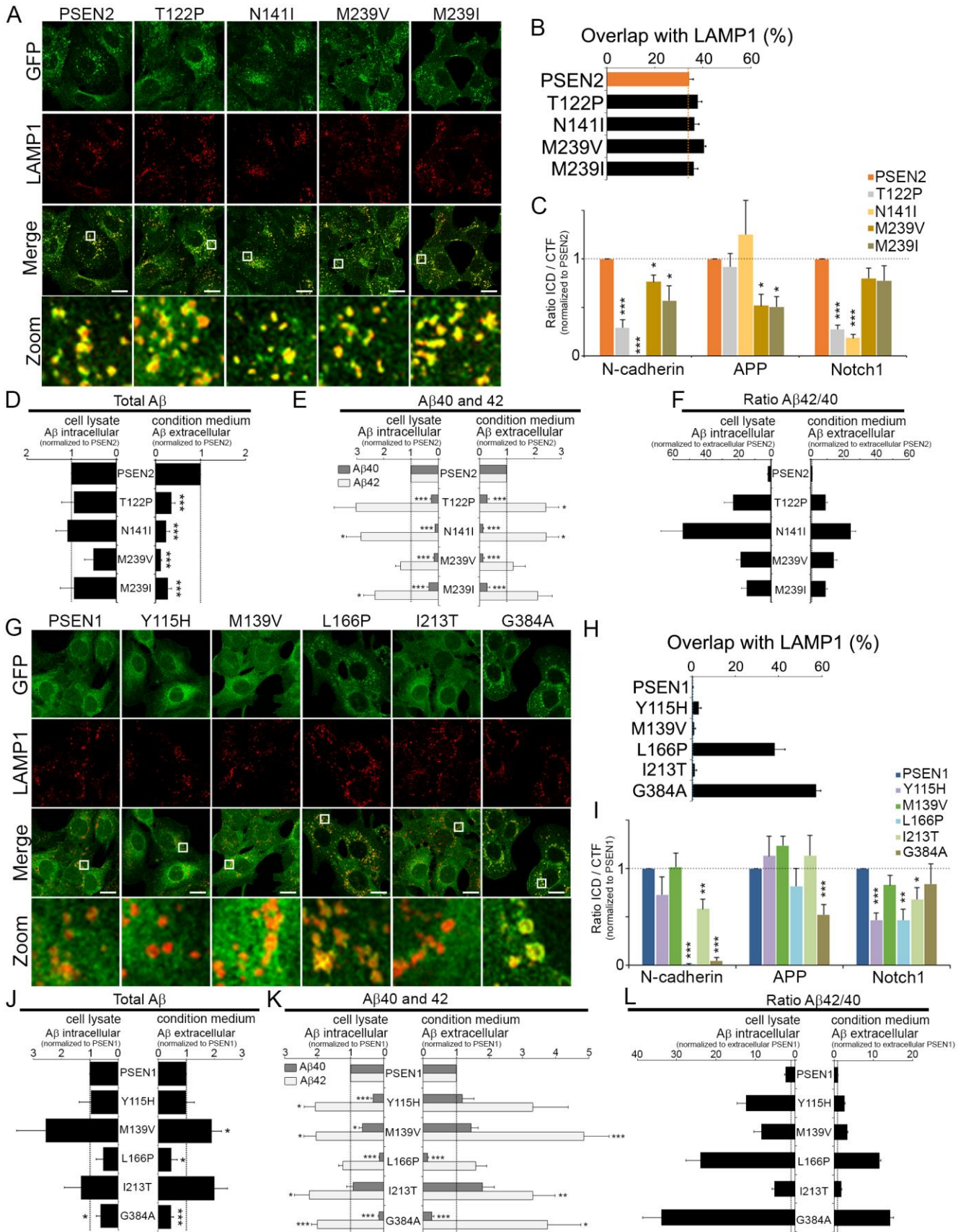
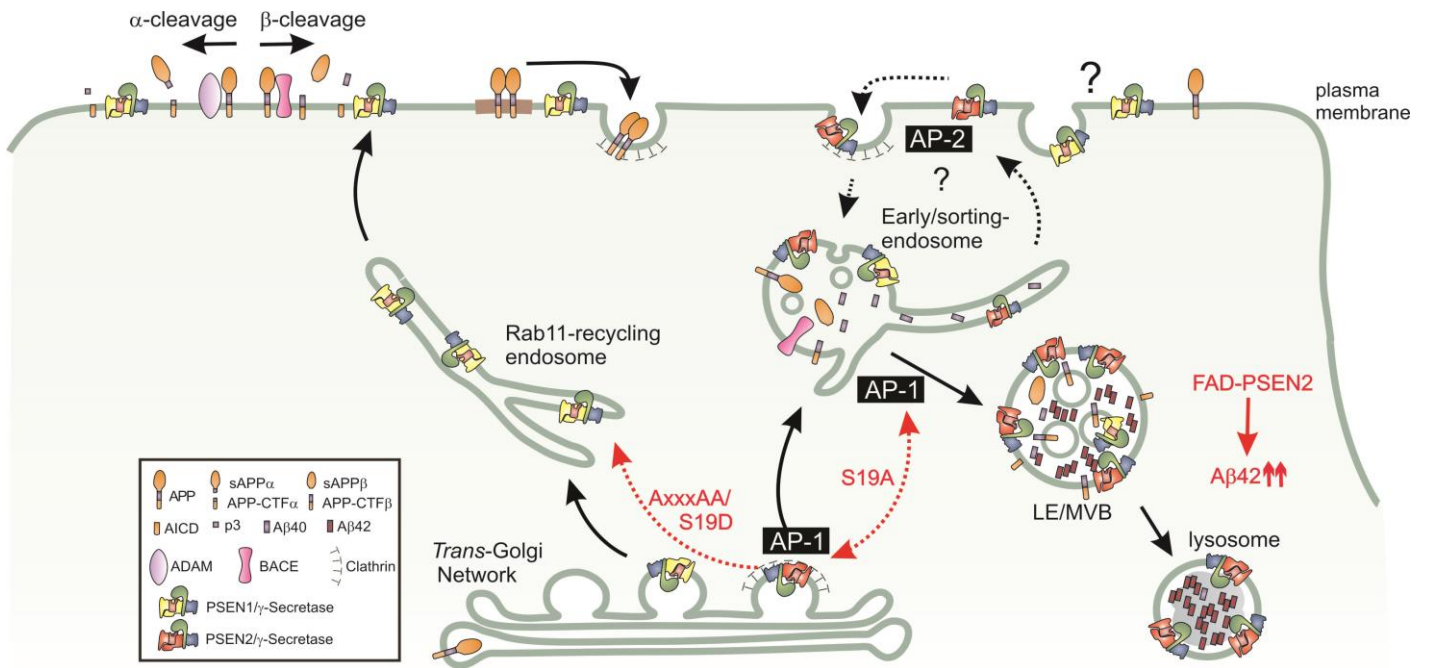


**FIGURE 7**



## Supplemental data

### FIGURE S1. Related to Figure 2

**Figure S1:** (A) Western blot analysis of total cell lysate (20  $\mu$ g protein) of different cell lines demonstrates high variability in endogenous PSEN1 and PSEN2 expression. Cancer cell lines derived from in particular melanoma (MNT-1), prostate (LNCaP) and lung carcinoma (22rv1, A549, 2427PT) have concomitant higher expression of PSEN2 and other subunits like mature NCT and PEN2 indicating higher  $\gamma$ -secretase complexes and activities.

(B-D) Differences in subcellular localization are recapitulated in (B) single PSEN1 and (C) single PSEN2 knockout MEF rescued with the respective GFP-tagged PSEN1 and PSEN2, as well as in (D) double knock out rescued with both GFP-PSEN1 and TagRFP-PSEN2. These results underscore that stable low exogenous expression of one PSEN does not influence subcellular distribution of the other. Insets: restricted distribution of GFP-PSEN2 and not GFP-PSEN1 in LAMP1-positive organelles. GFP-PSEN1 co-localizes with the ER-marker BIP in reticular patterns and with the transferrin receptor (TfR) at the cell surface. Bar= 10  $\mu$ m.

(E) Confocal analysis of isolated plasma membrane sheets prepared from MEF dKO double rescued cells (GFP-PSEN1 and TagRFP-PSEN2) shows that GFP-PSEN1 is more abundant at the cell surface than Tag RFP-PSEN2 complexes confirming cell surface biotinylation data (Figure 1). Lower panel represent a magnified view of the region represented by a square in the merged panel. Note the overall lack of co-localized spots suggesting that the different PSEN complexes exist in distinct microdomains. Bar= 10 $\mu$ m.

(F) Quantitative Western blot analysis of total cell lysate and LE/LYS magnetically isolated from single PSEN1 KO MEFs rescued with GFP-PSEN1 and single PSEN2 KO MEFs rescued with GFP-PSEN2. For both cell lines, endogenous PSEN2 as well as GFP-PSEN2 co-enriches with LAMP1. The ER-marker ribophorin is used as a negative control for the purification of LE/LYS. Data are the average of two experiments.

Related to Figure 1.

### FIGURE S2. Related to Figure 3

#### Figure S2:

(A) Y3H analysis shows that substitution of Leu for Met21 allows the PSEN2 tail to interact not only with AP1 $\gamma$ 1 $\sigma$ 1 but also with AP-2  $\alpha$ C $\sigma$ 2. In none of the occasions, interaction was detected with AP3 hemicomplexes.

(B) Western blot analysis of co-immunoprecipitations using anti-PSEN2 on CHAPSO extracts (150  $\mu$ g of total protein) from A549 and LNCaP cells. These cells were chosen because of their high endogenous PSEN2 expression levels. Endogenous AP1G1 (arrowhead) co-immunoprecipitates with PSEN2. \* Non-specific band that also is present in control lanes (bound fraction without anti-PSEN2).

(C) Western blot analysis (20  $\mu$ g total lysate/lane) of dKO MEFs stably rescued with GFP-PSEN2 mutants S<sub>19</sub>A, S<sub>19</sub>A, and AxxxAA with the indicated antibodies. All three PSEN2 mutants fully rescue NCT maturation and APP processing indicating restoration of  $\gamma$ -secretase activity.

(D) Graphical representation of the predicted effect on the interaction energy ( $\Delta\Delta G$ ) between the binding motif "CDERTSLMS" and the AP-1  $\gamma$ 1 $\sigma$ 1 hemicomplex while changing the Ser19 to all other amino acids. Note that next to Asp (D) also the phosphomimic Glu (E) as well as the structurally related Asn (N) give the highest positive  $\Delta\Delta G$ -values indicating that they are predicted to disfavor interaction.

(E) MS/MS spectrum of m/z 673,79 corresponding to mono-phosphorylated TSLMSAESPTSR after phosphorylation of GST-N<sub>1-86</sub>PSEN2 with Aurora kinase. The TSLMSAESPTSR peptide is shown to be phosphorylated (on S19 (as confirmed by a PhosphoRS 3.0 Site Probability of 99.7% and also by manual verification). Together with m/z 681,78 (RT 27,18 min), the oxidized methionine counterpart of this peptide, they are the only phosphorylated forms of the TSLMSAESPTSR peptide in this condition.

Related to Figure 3.

### FIGURE S3. Related to Figure 4

**Figure S3:** (A) MEF dKO rescued with either GFP-PSEN1 or GFP-PSEN2 were transiently transfected with Cherry-Rab5Q79L to block exit of endosomal cargo from early endosomes, fixed and processed for confocal microscopy. GFP-PSEN2 but not -PSEN1 co-accumulates with LAMP1 (white) in enlarged endosomes (merged inset) suggesting that GFP-PSEN2 is delivered to this early endosomal sorting compartment. Bar: 10  $\mu$ m.

(B) MEF dKO rescued with GFP-PSEN1, -PSEN2, hybrid PSEN proteins (hyb4 and hyb5, see Figure 2A) and -PSEN2 transport mutants (S<sub>19</sub>A, S<sub>19</sub>D and AxxxAA, see Figure 3A) were transiently transfected with Cherry-Rab11-wild type. Transient high overexpression of wild-type Rab11 causes the jamming of cargo like transferrin receptor (TFR). Co-accumulation of GFP-PSEN1 indicates that PSEN1 traffics through or via the Rab11-recycling compartment as opposed to GFP-PSEN2 which does not accumulate. Replacing the N-terminus of PSEN1 with the equivalent of PSEN2 (hyb4) results in a loss of Rab11 co-localization while reversely exchanging the N-termini of PSEN2 with the one of PSEN1 (hyb5) results in

co-accumulation. The S<sub>19</sub>A and S<sub>19</sub>D mutants of PSEN2 also fail to co-localize with exogenous Rab11. Instead, the AxxxAA mutant, which abrogates interaction with AP-1, now readily co-accumulates with the TFR in the Rab11 recycling compartment. This suggests that the AP-1 interaction prevents PSEN2 from being sorted via the Rab11 recycling compartment. Bar: 10 μm.

Related to Figure 4.

## FIGURE S4. Related to Figure 5

**Figure S4:** (A) Confocal analysis of MEF dKO rescued with GFP-PSEN2 (green) transiently expressing PMEL (red). Inset shows the localization of exogenous PMEL in GFP-PSEN2 positive endosomes. Bar=10μm. (B, B') MNT-1 cells transfected with Ctrl, PSEN1 or PSEN2 siRNA were analyzed 48 h later by western blot. Antibodies against the CTF part of PMEL and TRP1 were used to detect full-length and processed fragments. (B') is a long exposure of (B). PMEL-CTF and TRP1-CTF are the only fragments which accumulate upon downregulation of PSEN2. (C) PSEN1 and PSEN2 knockout MNT-1 cells were analyzed by Western blot. Antibodies against the CTF of PMEL, TRP1, and APP were used to detect full-length and processed fragments as indicated. P1: immature core-glycosylated PMEL form, Mβ: product of proprotein convertase cleavage; CTF: CTF fragment; FL: full-length. (D) EM analysis of epon-embedded RPE of WT and PSEN2-KO mice. Note the presence of normal ellipsoidal-shaped melanosomes in WT mice versus abnormal big round-shape melanosomes in PSEN2-KO mice (white arrows). Bar= 2 μm. (D') Ratio (marked as "R") between maximum width and length of an average of 150 melanosomes per condition. Melanosomes are significantly less elongated in PSEN2-ko RPE (\*\*P<0.01). (E) Delta ligand-induced processing of endogenous Notch1 in PSEN dKO MEFs rescued with GFP-PSEN1, -PSEN2 and transport mutants S<sub>19</sub>A, S<sub>19</sub>D and AxxxAA (see Figure 3A). Western blot analysis of the levels of Notch1- and Notch2-CTF and NICD production in the absence (-) and presence (+) of a γ-secretase inhibitor, DBZ (Dibenzazepine, 0.2 μM, 16 h). Note clear accumulation of the respective CTF fragments of endogenous Notch1 and Notch2 which are the substrates of γ-secretase. The cleaved NICD1 specific antibody (Val1744) only recognizes γ-secretase processed Notch1 but not Notch2. (E') Quantification of NICD production of Western blots in (E). No differences were found between PSEN1 and PSEN2, but the PSEN2-S<sub>19</sub>A decreased NICD production, while significantly more NICD is produced in the case of PSEN2-S<sub>19</sub>D expression (Mean ± SEM, n=3). (F) MEF dKO and rescued cell lines were transiently transfected with APP<sup>swedish</sup> (APP<sup>sw</sup>). After 24h, conditioned media were collected and cells were lysed. Total lysates (10 μg) were analyzed by Western blot to measure intracellular Aβ and transfection efficiency, and conditioned medium (25 μl) to evaluate secreted/extracellular Aβ levels.

Related to Figure 5.

## FIGURE S5. Related to Figure 6

### Figure S5:

(A and B) Western blot analysis of dKO MEFs stably rescued with (A) PSEN2-FAD mutants (T122P, N141I, M239V, M239I), and (B) PSEN1-FAD mutants (Y115H, M139V, L166P, I213T, G384A) displaying restored NCT maturation, PSEN2 stabilization and lack of APP-CTF accumulation underscoring rescued and normalized γ-secretase complex formation and activity.

(C and D) Quantification by ELISA of intracellular and extracellular Aβ<sub>40</sub> and Aβ<sub>42</sub> levels in the indicated patient primary fibroblast cells transiently transfected with C99-3XFLAG. For all quantification, Aβ signals were corrected for the level of C99-3XFLAG expression, and normalized to control 1 (mean ± SEM, n=6).

Note the selective strong increase of intracellular Aβ<sub>42</sub> and the Aβ<sub>42</sub>/40 ratio in the FAD PSEN2-N141I cell line.

Related to Figure 6.

## Legends to supplemental Movies: Related to Figure 4

### Supplemental Movie S1 related to Figure 4

SIM-CLEM of GFP-PSEN2-S<sub>19</sub>A-rescued dKO MEFs transiently overexpressing LAMP1-mCherry. A SIM image (x-y resolution ~125 nm; z-resolution ~300 nm) was superimposed on a stack of three consecutive EM transmission sections of 50 nm (total 150 nm). mCherry fluorescence was used as fiducial label to optimally position the SIM image on the organelles identified ultrastructurally as LE/LYS. The GFP-PSEN2-S<sub>19</sub>A fluorescence is clearly localized in tubules and clathrin-coated vesicles in close proximity to TGN stacks. One of the frames of this movie was used in Figure 4G'.

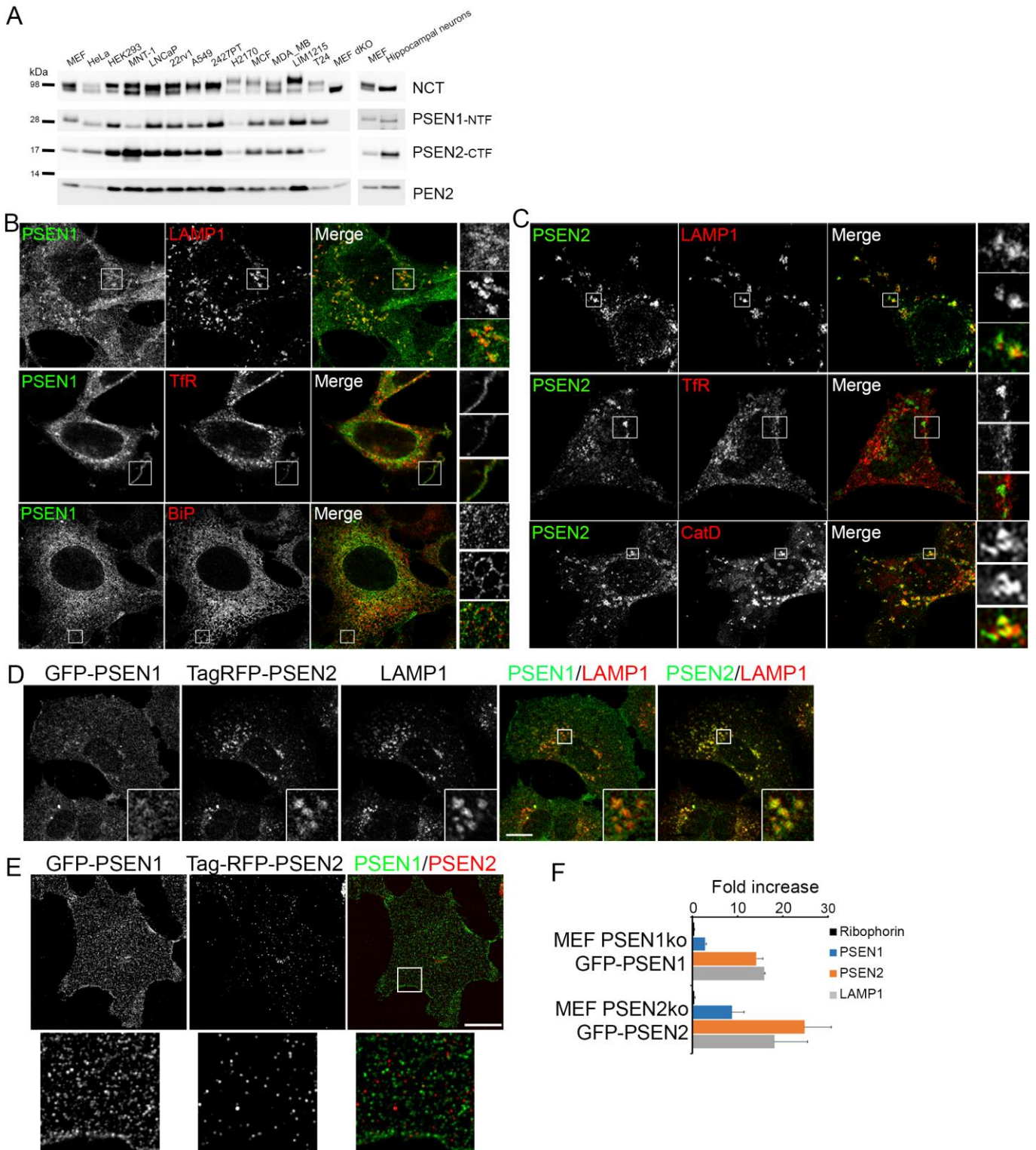
Related to Figure 4.

### Supplemental Movie S2 related to Figure 4

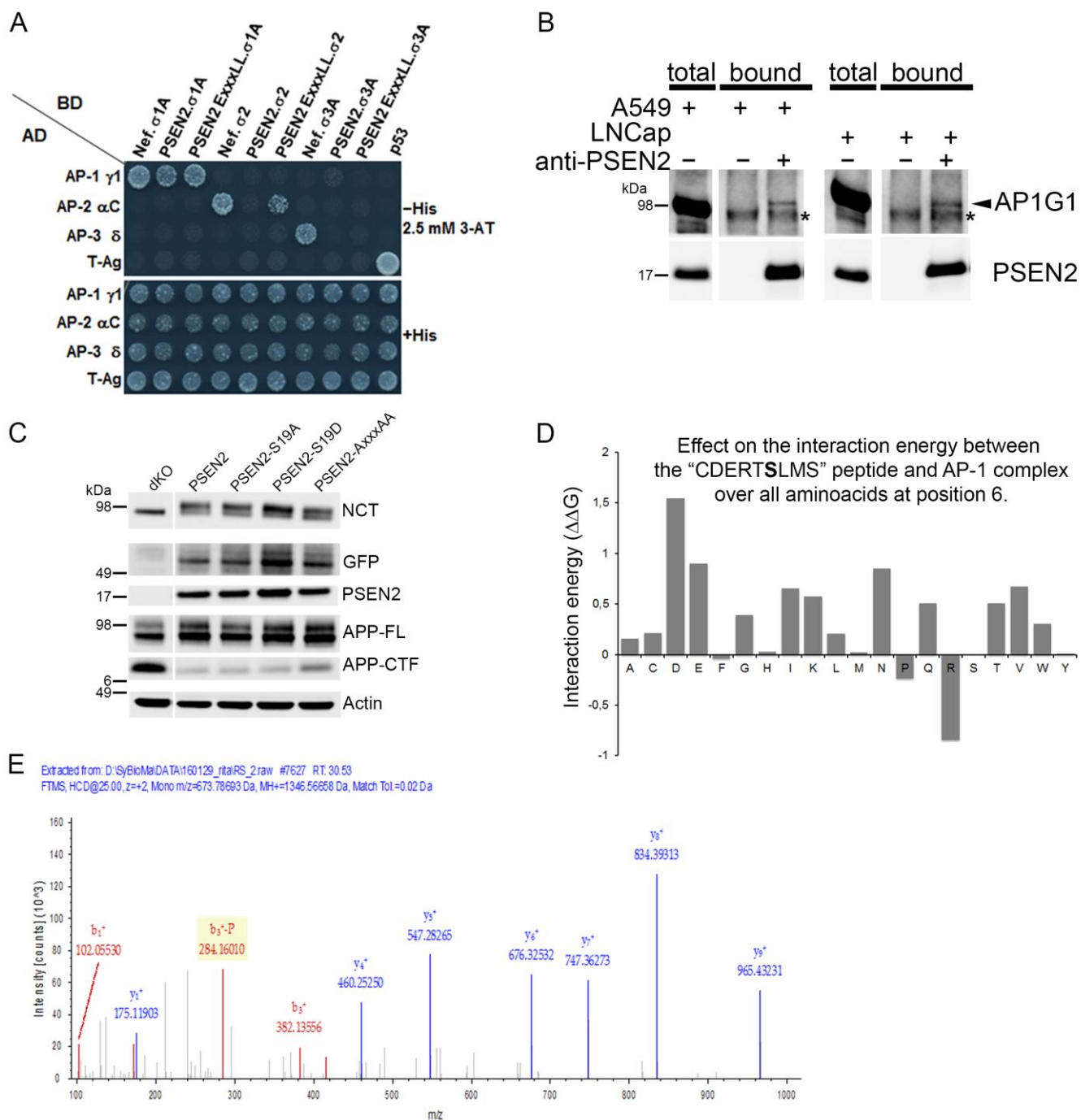
SIM-CLEM of GFP-PSEN2-S<sub>19</sub>A-rescued dKO MEFs stained with Mitotracker. A SIM-image was superimposed on a stack of eight consecutive EM transmission sections of 50 nm (total 400 nm). Mitotracker was used as fiducial marker to align the SIM

image with the mitochondria ultrastructure. The GFP-PSEN2-S<sub>19</sub>A fluorescence is concentrated in a rim neighboring several Golgi stacks. The presence of clathrin-coated vesicles and dilated tubules identifies this region as TGN. Related to Figure 4.

# Supplemental Figure S1

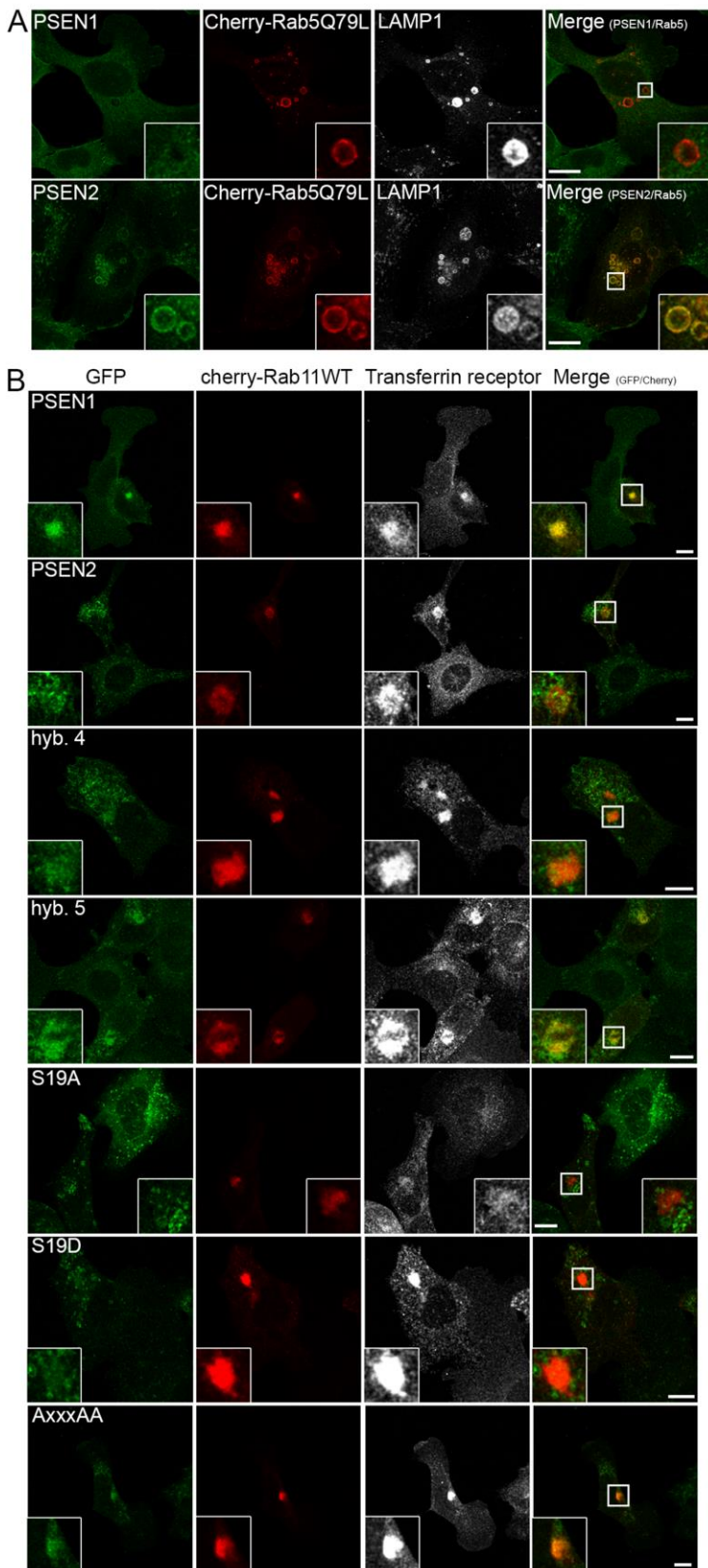


## Supplemental Figure S2

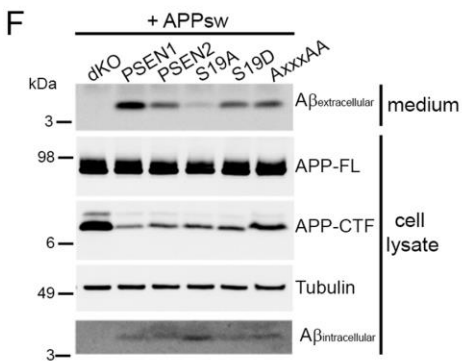
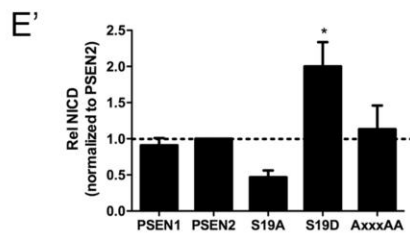
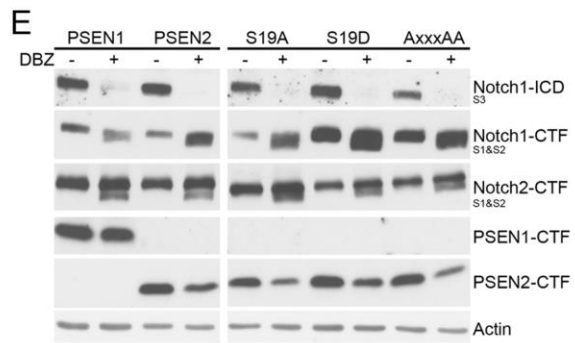
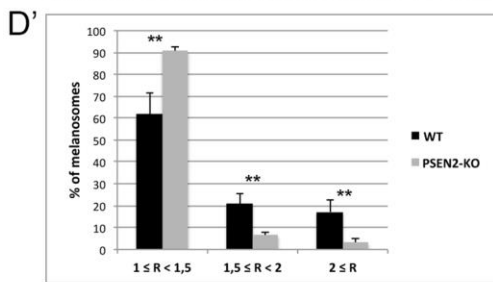
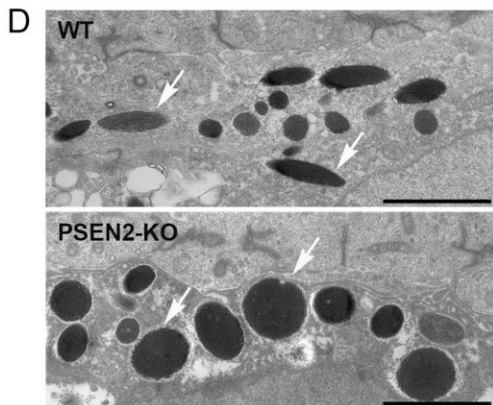
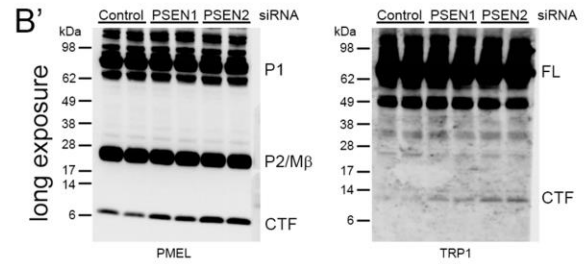
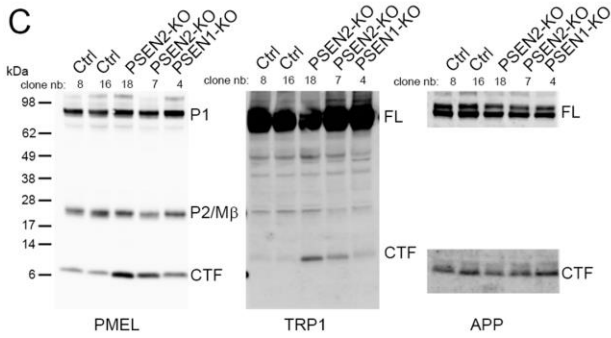
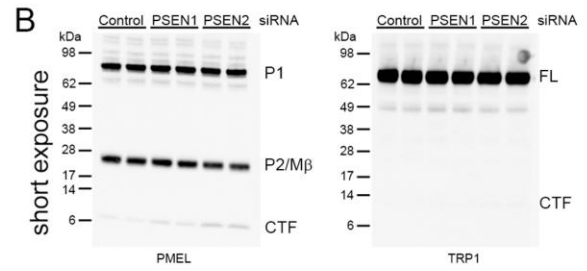
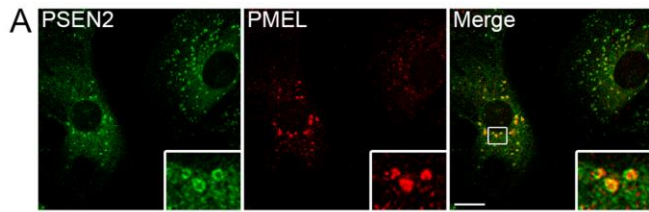




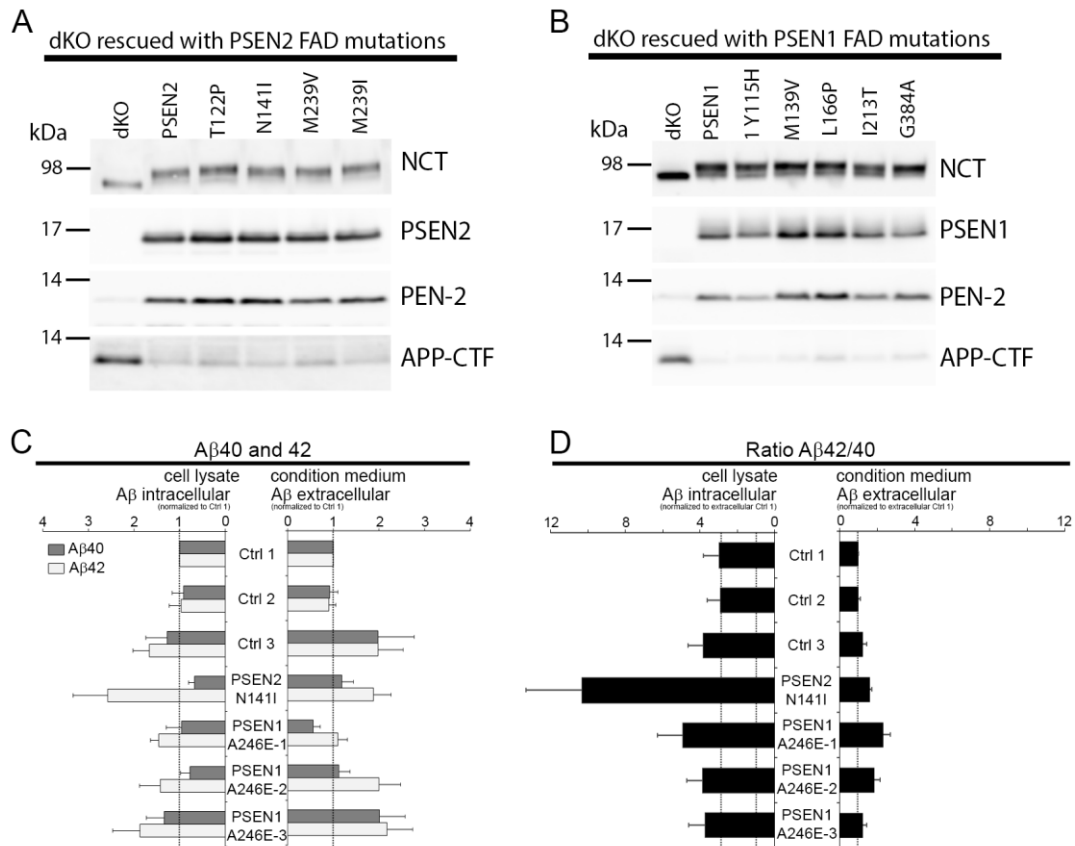
# Supplemental Figure S3



# Supplemental Figure S4



## Supplemental Figure S5



**Two Supplementary Movies:**

Movie-LAMP1-S19A-3sections

Movie2-Mito-S19A-8sections

## Supplemental Experimental Procedures

### Cell Culture, Generation of Stable Cell Lines and Primary Hippocampal Neuron Culture

All culture media and sera are from Life Technologies. Mouse embryonic fibroblasts (MEFs), wild-type (WT), PSEN1 and PSEN2 knock-out (dKO, (Herreman et al., 2000)), rescued dKO cell lines, HEK293, HEK293T, HeLa, A549, MCF7, MDA\_MB, T24 cells were routinely grown in Dulbecco's modified Eagle's medium (DMEM/F12) supplemented with 10% fetal calf serum (FCS). LNCaP, 22rv1, H2170 and LIM215 were grown in RPMI-1640 supplemented with 10% FCS. A549, MCF7, MDA\_MB, T24, LNCaP, 22rv1, H2170, LIM215 cells were kindly provided by J. Swinnen, KU Leuven, Belgium. The highly pigmented human melanoma MNT-1 cells were cultured in DMEM/Glutamax, with 10% AIM-V medium, 20% FBS, 1% non-essential amino acids (Raposo et al., 2001). All cell lines were maintained in a humidified chamber with 5% CO<sub>2</sub> at 37°C. Primary hippocampal neuron cultures are derived from E17-E18 mouse or rat embryos (Esselens et al., 2004). Stable rescued dKO cell lines were generated from MEFs dKO using replication-defective recombinant retroviral system (pMCSV vector, Clontech) expressing the gene of interest. Patient primary fibroblast cells were obtained from Coriell Cell Repositories: three PSEN1 FAD A246E: A246E-1(AG06840), A246E-2 (AG06848), A246E-3 (AG08711), three control: Ctrl 1 (AG07871), Ctrl 2 (AG08509), Ctrl 3 (AG08701) and one PSEN2 FAD-N141I (AG09908). These cells were cultured in DMEM/L-Glutamine with 15%FBS.

### Antibodies

The following monoclonal antibodies (mAbs) were commercially obtained: rat anti-LAMP1 (sc-19992, Santa Cruz); mouse anti-LAMP1 (BD Bioscience); mouse anti-transferrin receptor (TfR, clone H68.4, Life Technologies), anti- $\beta$ -actin (AC15, Sigma), anti-tubulin (DMIA, Sigma), anti-AP1G1 (clone 88, BD Bioscience), anti-AP3D1 (clone 18, BD Biosciences), anti-Tau-1 (Clone PC1C6, Chemicon); rabbit anti-AP2M1 (ab75995, abcam), human A $\beta$  AA 4-10 (WO2, the Genetics Company) and AA 1-16 (6E10, Signet Laboratories). The following polyclonal antibodies (pAbs) were purchased: rabbit anti-Rab11 (life Technologies), rabbit anti-PSEN1 (ab24748, abcam), rabbit anti-PSEN2 (ab51249, abcam), rabbit anti-Pen2 (ab18189, abcam) rabbit anti-AP1B1/AP2B1 (ab21981, abcam), rabbit anti-GFP (for immunoprecipitation, A-11122, Life Technologies), goat anti-GFP (for Western blot, 600-101-215, Rockland), chicken anti-GFP (for immunofluorescence, GFP-1020, aves Labs), rabbit anti-MAP2 (sc-20172, Santa Cruz), chicken anti-MAP2 (ab5392, abcam) rabbit anti-TRP1 (sc-25543, Santa Cruz), rabbit anti-PACS1 (ab56072, abcam), rabbit anti-TGN46 (ab16059, abcam), rabbit anti-EEA1 (sc-33585, Santa Cruz), rabbit anti-Notch1 (D1E11, Cell Signaling), rabbit-anti cleaved Notch1 (Val1744, Cell Signaling). The following antibodies were generously provided: mAb to Rab5 by (R. Jahn, MPI, Göttingen), pAb against Rab7 (P. Chavrier, CNRS, Paris), pAb against Ribophorin (R. Schekman, Berkeley, US), pAb against Cathepsin D (P. Saftig, Institut of Biochemistry, Kiel). Rabbit pAb against APP C-terminus (B63.3), PSEN1-NTF (B19.3), PSEN2-CTF (B24), PEN-2 (B126.1) and mAb against NCT (9C3) were generated in-house (Annaert et al., 1999; Esselens et al., 2004; Herreman et al., 2003). Affinity purified anti-peptide antibody recognizing the C-terminus of PMEL was previously described (Raposo et al., 2001). ELISA antibodies were obtained through collaboration with Janssen Pharmaceutica NV, Beerse, Belgium: JRF/cAb40/28 for A $\beta$ 1-40, JRF/cAb42/26 for A $\beta$ 1-42, and detection antibody JRF/AbN/25 against the N terminus of A $\beta$ .

### Plasmids, Transfection, RNAi

The plasmids pSG5-C99-3xFLAG and pcDNA-APPsw (Swedish mutant of APP) were previously described (Bentahir et al., 2006; Sannerud et al., 2011) respectively. cDNAs encoding human WT PSEN1 and PSEN2 were cloned into pEGFP-C1 between EcoRI and BamHI restriction sites. GFP-PSEN1 and GFP-PSEN2 sequences were digested with AfeI and HpaI, and inserted into the HpaI linearized pMSCV-puro (Clontech). pTagRFP-PSEN2 were obtained (Evrogen). For lentivirus infection of neurons, EGFP-PSEN1 and EGFP-PSEN2 inserts were cut out from pEGFP-PSEN1-C1 and pEGFP-PSEN2-C1 using NheI/XbaI restriction sites and ligated into a lentiviral plasmid pFUGW cut with XbaI. cDNAs encoding GFP fused to PSEN1 and PSEN2 hybrids (Zhao et al., 2008) were cloned into pMSCV for virus production. The hybrids were named as such: Hyb. 1: (1-268(PSEN1), 275-304(PSEN2), 299-467(PSEN1)); hyb. 2: (1-298(PSEN1), 305-355(PSEN2), 375-467(PSEN1)); hyb. 3: (1-298(PSEN1), 305-448(PSEN2)); hyb. 4: (1-76(PSEN2), 71-467(PSEN1)); hyb. 5: (1-70(PSEN1), 77-448(PSEN2)). GST-N<sub>1-81</sub>PSEN1-NTF and GST-N<sub>1-86</sub>PSEN2 were generated previously (Annaert et al., 2001). Mutations in PSEN2 were introduced using QuickChange II Site-Directed Mutagenesis Kit (Agilent Technologies) according to the manufacturer with the forward primers: S19A: 5'-gtgatgagcggacggccctaatgtcgcc-3'; S19D: 5'-gtgtgatgagcggacggacctaataatgtcgccgag-3'; S7A-S9A (named SSAA) 5'-ctcacattcatgcccgtgacgcccaggaagaagtgtgtg-3'; S7D-S9D (named SSDD): 5'-ctcacattcatgcccgtgacgcccaggaagaagtgtgtg-3'; E16A-L20A-M20A (named AxxxAA): 5'-gtgtgtgatgcccggacgtcgcgctgcccagagagccc-3' and there reverse complement. Mutations in GST-N<sub>1-86</sub>PSEN2 were generated using the following primers: S19A: 5'-gtgatgagcggacggccctaatgtcgcc-3'; S19D: 5'-gtgtgatgagcggacggacctaataatgtcgccgag-3'; S7A-S9A (named SSAA) 5'-tggtgacattcatgcccgtgacgcccaggaagaagtgtgtg-3'; S7D-S9D (named SSDD): 5'-caccatggtgacattcatgcccgtgacgcccaggaagaagtgtgtg-3'; E16A (named AxxxLM): 5'-gaagaggtgtgtgatgcccggacgtccttgatg-3'; M21A (named ExxxLA): 5'-agcggacgtccttgccgctcagcccagagcc-3'; E16A-L20A-M20A (named AxxxAA): 5'-agaggtgtgtgatgcccggacgtcgcgcccagagagcc-3' and there reverse complement. PSEN1-FAD mutations were generated using the following primers: Y115H: 5'-gatggcagctaatacattccattcac-3'; M139V: 5'-gaatgctgccatgctgatcagtgctattg-3'; L166P: 5'-ggatcatcatgctgctattatcatctc-3' I213T: 5'-gggaatgattccactcactgaaaggtcc-3'; G384A: 5'-cttgattgagcagattcttctacagtttctgtg-3'; and there reverse complement. PSEN2-FAD mutations were generated

using the following primers: T122P: 5'-gacagctcatctaccgccattcactgag-3'; N141I: 5'-caactcctgctgatcacctcatcatg-3'; M239V: 5'-cagtgcgctcgtggccctagtgttc-3'; M239I: 5'-gatcagtcgctcattgccctagtgttc-3'; and their reverse complement. All constructs were verified by sequencing.

Cells were transfected with EugeneHD (Roche Diagnostics) to express C99-3xFLAG. Primary hippocampal neurons were infected at 3 to 4 days in vitro (DIV) and analyzed at 7 DIV.

The siRNAs targeting human PSEN1 (L-004998), human PSEN2 (L-006018) and non-targeting control (D-001810) ON-TARGETplus SMARTpool were from Thermo Scientific. siRNA transfections were performed using JetPRIME (Polyplus transfections) and analyzed 72h after down-regulation.

Plasmid to express LAMP1-mCherry is from addgene (#45147).

### **Virus Production**

For virus production, HEK293T cells were transiently transfected using FuGENE6 (Promega) according to the manufacturer instruction. For retrovirus packaging, pMSCV expressing the gene of interest was cotransfected with the helper plasmid pIk (Ecopac). Lentiviral particles were produced by co-transfection of appropriate lentiviral vectors with packaging (pCMV- $\Delta$ R8.74) and envelope (pMD2.G) plasmids in HEK293T cells. Plasmids pFUGW, pCMV- $\Delta$ R8.74 and pMD2.G were a gift of Y. Arsenijevic (University of Lausanne, Jules-Gonin Eye Hospital, Lausanne, Switzerland). Lentiviral Particles were purified by ultracentrifugation and resuspended in DMEM/F12 medium.

For transduction, viral particles were diluted in medium containing Polybrene (8 ng/ $\mu$ l, Sigma). After 24 h, medium was refreshed. To establish stable cell lines, transduced cells were selected using 5  $\mu$ g/ml puromycin (Sigma).

### **Western blot**

Protein concentrations were determined by the Bio-Rad DC protein assay (Bio-Rad). Samples were separated by SDS-PAGE (4-12% Bis-Tris NuPAGE gels in MES running buffer (Life Technologies) and transferred onto nitrocellulose membranes (Life Technologies). After blocking in 5% non-fat milk, membranes were incubated with primary antibody (4°C, overnight) followed by washing and incubation with horseradish peroxidase (HRP)-conjugated secondary antibodies (1h, room temperature). After final washing, immunodetection was done using enhanced chemiluminescence (Western Lightning-Plus ECL, PerkinElmer), and immunoreactive protein bands were digitally captured and quantified on a Fuji MiniLAS 3000 imager (Fuji, Düsseldorf, Germany) using Aida Image Analyzer software (Raytest, Germany). Data are represented as mean  $\pm$  SEM of at least three independent experiments.

### **Discontinuous Sucrose/D<sub>2</sub>O Flotation Gradient**

For each gradient, two 600cm<sup>2</sup> tissue culture plates of confluent MEFs were used. All steps were carried out at 4°C and performed as described (Gorvel et al., 1991) with some modifications. Briefly, cells were scraped in ice-cold PBS Dulbecco's and centrifuged (5 min, 650xg). Cell pellets were resuspended in 2 ml homogenization buffer (250 mM sucrose, 3 mM imidazole, pH=7.4), and homogenized using a cell cracker (4 passages, clearance 10  $\mu$ m, Isobiotec, Germany). Protease inhibitors (PI, cOmplet Protease Inhibitor Cocktail tablet from Roche) were added and after a brief centrifugation (10 min at 800xg) a post-nuclear supernatant (PNS) was brought to 40.6% sucrose and loaded on the bottom of a centrifugation tube and overlaid with 3,7 ml 16% sucrose, 3 ml 10% sucrose (in D<sub>2</sub>O, 3 mM imidazole, pH=7.4, 0.5 mM EDTA) and finally 1.5 ml homogenization buffer. After centrifugation (1.4h, at 151,263xg) in an SW41 rotor, twelve 1ml fractions were collected and equal amounts of protein were used for Western blotting and  $\gamma$ -secretase assays.

### **Isolation of Late Endosomes/Lysosomes (LE/LYS)**

LE/LYS were isolated according to (Tharkeshwar et al., submitted). Cells (90% confluency) were incubated (Pulse) with DMSA-coated SPIONs suspended in culture medium (concentration 0.2 mg/ml) for 15 min at 37°C. After a wash with PBS, cells were re-incubated (Chase) at 37°C in fresh medium for 240 min, followed by three successive washes with acidic buffer (0.15M glycine, pH 3), cold PBS and harvested by scraping, centrifugation (180 g, 10 min) and resuspension in homogenization buffer (HB; 250 mM sucrose, 5 mM Tris and 1 mM EGTA pH 7.4 supplemented with PI). After cell cracking (12 passages, clearance 10 $\mu$ m) the total homogenate was centrifuged (800xg, 10 min) and the PNS loaded on a LS column (pre-equilibrated with HB) placed in a strong magnetic field (0.5 T) (SuperMACSII, Miltenyi). The hydrophilic matrix of the LS column enhances retainment of SPIONs along with its adhering subcellular compartments, allowing nonmagnetic material to be removed by extensive washes with ice-cold HB. Next, the column was detached from the magnetic field and the bound fraction containing LE/LYS was eluted using HB, centrifuged (126,000xg, 1 h) and the resulting pellet re-suspended in 200  $\mu$ l HB. Equal amounts of protein were denatured in sample buffer (Life Technologies), and analyzed by Western blot. Each experiment was performed two to three times.

### **Cell Surface Biotinylation**

Cell surface biotinylation was performed as described (Sannerud et al., 2011). Briefly, cells were placed on ice, washed in PBS (pH=8) and incubated in PBS (pH=8) supplemented with 0.25mg/ml sulfo-NHS-SS-Biotin (Pierce) (10min at 4°C). Excess of biotin was washed out and remaining biotin quenched with 1% BSA in PBS (15min at 4°C). Cells were lysed in lysis buffer (50mM HEPES, pH 7.2, 100mM NaCl, 1% Triton X-100, with PI). Total protein was measured and biotinylated proteins were pulled down from equal amounts of extracts using streptavidin Sepharose beads (Pierce) (4°C, 2h on a rotation wheel). After washing, bound material was eluted from the beads using 2x loading buffer (Life Technologies) containing 2%  $\beta$ -

mercaptoethanol (70°C for 10 min), and analyzed by Western blot. Each experiment was performed at least three times. Values are presented as mean  $\pm$  SEM.  $\beta$ . P values were determined by Student's *t*-test, unpaired, unequal variance ( $*p<0.05$ ,  $*p<0.01$ ,  $***p<0.001$ ).

### Co-Immunoprecipitation (Co-IP)

Cells were harvested in ice cold PBS+/. After centrifugation (1,700 $\times$ g for 5 min, 4°C) cell pellets were resuspended in lysis buffer (50 mM Hepes, pH 7.4, 150 mM NaCl, 1% CHAPSO, PI). After 1 h at 4°C, lysates were centrifuged (20,000 $\times$ g, 15 min, 4°C) and total protein was measured from the supernatant. The same amount of protein (500  $\mu$ g) was incubated with 1.5  $\mu$ l of rabbit anti-GFP, or rabbit anti-PSEN2 for 2 h at 4°C, followed by incubation with protein-G (20  $\mu$ l) overnight at 4°C, under constant rotation. The immune complexes were washed three times with lysis buffer, once with 0.5 $\times$  Tris-buffered saline (TBS, 1 $\times$ : 10 mM Tris, 150 mM NaCl, pH =7.4), then denatured in 18  $\mu$ l of sample buffer and analyzed by Western blot. Total lysate (20  $\mu$ g) was used as input. Blots were probed as indicated in the Figures.  $\beta$ . Each experiment was performed at least 3 times. Values are presented as mean  $\pm$  SEM. P values were determined by Student's *t*-test, unpaired, unequal variance ( $*p<0.05$ ,  $*p<0.01$ ,  $***p<0.001$ ).

### A $\beta$ detection

Cells were processed 24 h after transfection with C99-3 $\times$ FLAG (or APP<sub>sw</sub>). Conditioned medium were collected and cell debris were removed by centrifugation. Cells were washed twice with PBS+ and lysed in lysis buffer (50 mM Tris-HCL, pH 7.4; 150 mM NaCl, 1% Triton X-100; 0.1% SDS; 0.5% sodium deoxycholate; PI).

#### For total A $\beta$ detection:

Equal volume of conditioned medium (3% of total volume, A $\beta$  extracellular pool) and equal amount of total protein (10  $\mu$ g, A $\beta$  intracellular pool) from cell lysate were analyzed by western blot. For each cell line, A $\beta$  signals (extracellular and intracellular) were quantified and corrected for C99 expression level.

#### For A $\beta$ 40 and 42 quantification, ELISA:

A $\beta$ 40 and 42 were measured in conditioned medium (3% of total volume, extracellular pool) and in cell lysate (10  $\mu$ g, intracellular pool) by ELISA. 96-well MSD plates were coated with anti-A $\beta$ 40 or -A $\beta$ 42 antibodies overnight. After rinsing 5 $\times$  with washing buffer (PBS +0.05% Tween-20), plates were blocked with 150  $\mu$ l/well 0.1% casein buffer for 1 h at room temperature (600 rpm) and rinsed 5 $\times$  with 150  $\mu$ l/well washing buffer. 25  $\mu$ l SULFO-TAG JRF/AbN/25 detection antibody diluted in blocking buffer was mixed with 25  $\mu$ l of standards (synthetic human A $\beta$ 1-40, and A $\beta$ 1-42 peptides) or reaction samples diluted in blocking buffer and loaded 50  $\mu$ l per well. After overnight incubation at 4°C, plates were rinsed with washing buffer and 150  $\mu$ l/well of the 2 $\times$  MSD Read Buffer T (Tris-based buffer containing tripropylamine, purchased from Meso Scale Discovery) was added. Plates were immediately read on a Sector Imager 6000 (Meso Scale Discovery). We determined the amount for A $\beta$ 40, and A $\beta$ 42 and corrected it for the C99 expression level and normalized to PSEN1 or PSEN2 as indicated. Ratio 42/40 were normalized to PSEN1 or PSEN2 as indicated, but to the secreted pool in order to compare secreted versus cellular pool of A $\beta$ . Each experiment was performed at least 3-6 times. Values are presented as mean  $\pm$  SEM. P values were determined by Student's *t*-test, unpaired, unequal variance ( $*p<0.05$ ,  $*p<0.01$ ,  $***p<0.001$ ).

### GST-Assay

The cDNAs encoding GST fused to the first 81 and first 86 amino acids of PSEN1 and PSEN2, respectively, were subcloned into pGEX4T-1, transformed in *E. coli* BL21. Recombinant GST fusion proteins were induced using 0.1 mM IPTG for 2 h at 30°C and extracted and purified as described (Annaert et al., 2001). Briefly, *E. coli* pellets were resuspended in Tris-saline buffer (150 mM NaCl, 10 mM Tris, pH 7.4), sonicated and further extracted with Triton X100 (15 min). The cleared extracts (20 min, 16,000 $\times$ g) were mixed with glutathione coupled to Sepharose (GE healthcare) 30 min, 4°C). After extensive washing, beads were incubated overnight with extracts of brain cortexes of C57 black p1 pups. Extraction of cortexes was performed in PBS-/-, 1% Triton X-100 supplemented with PI. The next morning beads were washed 4 $\times$  in PBS-/- with 1% Triton X-100 and PI and once with 0.3 $\times$  TBS. Bound material was eluted with 4 $\times$  sample buffer and processed for SDS-PAGE and Western blot.

### Notch ligand stimulation and immunoblotting

Cells were plated on rDII4-Fc (1 $\mu$ g/ml; R&D Systems) coated plates and treated with DMSO or Dibenzazepine (DBZ; 0.2  $\mu$ M; Syncom, Groningen, The Netherlands) for 16 h. Cells were directly lysed in Laemmli buffer prior to resolving by SDS-PAGE. Proteins were transferred onto nitrocellulose membranes and blocked for 1 h in 5 % skim milk in PBS, 0.05 % Tween-20 (PBS-T). Membranes were probed overnight at 4°C with primary antibodies and bound antibodies were visualized using HRP-linked secondary antibodies (Cell-Signaling) and ECL Luminescence (Pierce Biotechnology). Anti-Notch1 antibody (D1E11, 1:1000), anti-NOTCH2 antibody (D76A6, 1:2000), anti-cleaved Notch1-Val1744 antibody (D3B8, 1:1000) and anti-Presenilin 2 antibody (2192, 1:1000) were purchased from Cell signaling. Anti-Presenilin 1 antibody (1:1000) was purchased from Chemicon and anti- $\beta$ -actin antibody was purchased from MP Biomedicals.

### Yeast three-hybrid

**DNA constructs:** BamHI/PstI fragments encoding either wild-type, E16A, S19A, S19D, M21A or E16A/L20A/M21A mouse PSEN2 cytosolic tail (residues 1-87) were amplified from the corresponding constructs in pGEX-4T1. These fragments were subcloned into the BamHI/PstI sites of the multiple cloning site (MCS) 1 of pBridge (Clontech) vector-based constructs containing cDNAs encoding either human  $\sigma$ 1A, rat  $\sigma$ 2 or human  $\sigma$ 3A in their MCS2 (generating pBridge-PSEN2 tail. $\sigma$ 1A,

pBridge-PSEN2 tail.σ2 and pBridge-PSEN2 tail.σ3A plasmids). The pBridge-PSEN tail M21L.σ1A, pBridge-PSEN tail M21L.σ2 and pBridge-PSEN tail M21L.σ3A plasmids were generated by site-directed mutagenesis (QuickChange, Agilent) of the wild-type constructs. All constructs were verified by sequencing. The pGADT7 (Clontech) vector-based constructs encoding mouse AP-1 γ1, rat AP-2 αC or human AP-3 δ subunits were previously described (Janvier et al., 2003; Mattera et al., 2011).

**Yeast three-hybrid (Y3H) analysis:** Assays were performed using the HF7c reporter strain as described (Janvier et al., 2003; Mattera et al., 2011). Double transformants were selected in medium lacking leucine, tryptophan and methionine but containing histidine (+His), while interactions were assessed in the same medium lacking histidine (-His). The positive and negative controls used in the assays are described in the corresponding figure legend.

### **γ-Secretase Activity Assay**

Assays using recombinant substrate (Figure 1). Equal amount of total protein (7.5 μg) of each fraction was resuspended in 15 μl TE buffer (5 mM Tris-HCl, 1 mM EDTA, pH=7.0) containing 0.5% CHAPS and incubated for 1 h at 4°C. Extracts were incubated overnight at 37°C with 1 μl recombinant APP-C100-FLAG (Li et al., 2000), 1 μl DMSO and 1 μl 1M Tris-HCl pH=7.0. De novo formed Aβ was analyzed by Western blot (WO-2 mAb).

Assay with endogenous substrates (Figure 5 and 6). All procedures were carried out at 4°C. Cells (80% confluent) were washed twice with ice cold PBS and scraped. After centrifugation (600xg, 5 min), cells were resuspended in 750 μl hypotonic buffer (10 mM Tris pH 7.6, 1 mM EDTA, 1 mM EGTA) supplemented with PI and incubated on ice for 15 min. After centrifugation (20,000xg, 10 min) to remove cell debris, protein concentration of the supernatant was measured and four aliquots of 60 μg were again centrifuged (20,000xg, 60 min). Pellets were resuspended into 15 μl citrate buffer (150 mM sodium citrate, pH=6.4); three samples, from which one was supplemented with 1 μM DAPT (control), were incubated at 37°C for 3 h, and one was kept at 4°C (starting material). The assay was stopped after three h by adding 5 μl of 4x loading buffer followed by heating (10 min, 70°C), loaded for SDS-PAGE and analyzed by Western blot. Proteolytic activity was quantified using a C-terminal antibody washed in PBS (pH=8) and incubated in PBS (pH=8) supplemented with 0.25 mg/ml sulfo-NHS-SS-Biotin (Pierce) (10min at 4°C). Excess of biotin was washed out and remaining biotin quenched with 1% BSA in PBS (15min at 4°C). Cells were lysed in lysis buffer (50mM HEPES, pH 7.2, 100 mM NaCl, 1% Triton X-100, with PI). Total protein was measured and biotinylated proteins were pulled down from equal amounts of extracts using streptavidin Sepharose beads (Pierce) (4°C, 2h on a rotation wheel). After washing, bound material was eluted from the beads using 2x loading buffer (Life Technologies) containing 2% β-mercaptoethanol (70°C for 10 min), and analyzed by Western blot. Each experiment was performed at least 3 times. Values are presented as mean ± SEM. P values were determined by Student's *t*-test, unpaired, unequal variance (\**p*<0.05, \*\**p*<0.01, \*\*\**p*<0.001).

### **Mouse brain section**

Brain sections were prepared as described in Rubio et al (Rubio et al., 2012). Briefly, CD-1 mice (P10 days) were deeply anesthetized and perfused with 4% paraformaldehyde in phosphate buffer. The brains were cryoprotected, frozen, and 30-μm sections were cut. Coronal sections were stored in a cryoprotectant solution (30% glycerin, 30% ethylene glycol, and 40% phosphate buffer) at -20°C until use.

### **Immunohistochemistry:**

Tissue specimens were permeabilized in PBS+/+ containing 0.2% Triton X-100 and then incubated in blocking buffer (10% goat serum, 0.2 M Glycine, 0.2% Triton-X100, 0.2% gelatin, in PBS+/+) for 2h. Primary antibodies, diluted in blocking buffer were incubated with the specimens overnight at 4C. After few washes in PBS containing 0.2% Triton X-100, sections were incubated with secondary antibodies diluted in blocking buffer, for 1h. After few washes, sections were mounted in Mowiol.

### **Confocal Laser Scanning Microscopy and Quantification**

Cells were plated on glass coverslips, transfected 24 h later and processed for indirect immunolabeling the next day (Sannerud et al., 2011). Images were captured on a confocal microscope (Leica TCS SP5 II, Leica Microsystems) connected to an upright microscope, using an oil-immersion plan Apo 60x A/1.40 NA objective lens. Image acquisition was performed with LAS (Leica Microsystems). For live imaging of neurons treated with LysoTracker Red DND-99 (50 mM, Thermo Fisher Scientific), images were captured at 37°C on a Nikon A1R confocal system connected to an inverse microscope (Ti-2000; Nikon) using an oil-immersion Plan-Apochromat 60× A/1.40 NA objective. Data were collected using Nikon Imaging Software and further processed with ImageJ and PhotoshopCS6 (Adobe, CA).

ImageJ software with the plugin JACoP (Bolte and Cordeliers, 2006) was used for signal overlap quantification (Mander's coefficient). Images were acquired with identical settings and regions of interest (ROI) covering whole cells were used for quantification. Data are represented as Mean ± SEM for 8 to 15 cells in three independent experiments). Dendrite/axon polarity index (D/A) of PSEN1, PSEN2 WT and mutants (AxxxAA, S19D and S19A, Figure 6C') were calculated in neurons expressing PSEN1 or -2 and immunostained for MAP2 (to label dendrites) and Tau1 (to label axons). Images were acquired with identical settings. Several ROIs were drawn along neurites (dendrites or axons) within a field of view containing one or two neurons expressing PSEN1 or -2. For each ROI Mander's coefficients were measured for GFP:MAP2 and GFP:tau1. For each ROI the polarity index corresponding to the ratio GFP:MAP2 /GFP:tau1 was calculated and represented as mean ± SEM. P values were determined by Student's *t*-test, unpaired, unequal variance (\**p*<0.05, \*\**p*<0.01, \*\*\**p*<0.001).

### **Electron microscopy**



For conventional EM of MNT-1 cells, cells grown on coverslips were processed for Epon embedding and ultrathin sections and then contrasted with uranyl acetate and lead citrate as described previously (Raposo et al., 2001).

For conventional EM analysis of RPE sections, tissue blocks (eyes) from *Psen2*<sup>-/-</sup> mice (maybe you need to describe more, background and age for example) and WT mice were processed for Epon embedding and ultrathin sections and then contrasted with uranyl acetate and lead citrate as described previously (Lopes et al., 2007).

All samples were analyzed by using a FEI Tecnai Spirit electron microscope (FEI Company), and digital acquisitions were made with a numeric camera (Quemesa; Soft Imaging System).

Image Analysis and Quantification. Melanosome stages were defined by morphology (Raposo et al., 2001; Seiji et al., 1963). Quantification of melanosomes was determined by using iTEM software (Soft Imaging System).

### **Correlated light and electron microscopy (CLEM)**

The MEF dKO rescued with GFP-PSEN2-WT or GFP-PSEN2-S<sub>19</sub>A were plated on glass bottom dishes (MatTek). Cells were either expressing LAMP1-mCherry (24h transient expression) or labeled with MitoTracker (100 nM, 30 min, Thermo Fisher Scientific). Cells were fixed first by adding 1 ml pre-warmed double strength fixative solution (7% paraformaldehyde, 0,4% glutaraldehyde in 0,1 M phosphate buffer) to the medium while rotating at room temperature. After 10 min solution was replaced by single strength fixative solution (4% paraformaldehyde, 0,2% GA in 0,1M phosphate buffer). Cells were kept in this fixative solution in the dark until imaging (up to 1 h).

#### Super resolution light microscopy:

Structured illumination microscopy was used as a technique for super resolution light microscopy. An inverted Zeiss Elyra equipped with a stage for mounting dishes was used. During SIM imaging the cells were maintained in PBS <sup>-/-</sup>. To be able to correlate the same cells in light and electron microscopy, two marks were drawn on the bottom of the glass coverslips with a distance of 5 mm.

Nicely spread single cells, expressing GFP-PSEN2 (WT or S<sub>19</sub>A mutant) together with LAMP1-mCherry or MitoTracker, near one mark, were identified. Once found a cell of interest both transmitted light and fluorescence z-stack SIM images were taken using the 63x objective. The z-stack slices have a 0.2 μm thickness. After light imaging, the PBS <sup>-/-</sup> was replaced by a fixative solution of 2.5% GA in 0.1 M sodium cacodylate buffer. The cells were kept in this fixative solution overnight at 4°C.

#### Preparation for TEM:

Cells were washed three times in 0.1 M sodium cacodylate buffer. To enhance EM membrane contrast, cells were first treated with 2% osmium tetroxide in 0.1 M cacodylate buffer for 1 h, next with 1 % tannic acid dissolved in 0.1 M cacodylate buffer for 30 min, followed by 1 % osmium tetroxide in 0.1M cacodylate buffer for 30 min. All steps were done at room temperature with 0.1 M sodium cacodylate washing steps in between.

The cells were then dehydrated in solutions of ethanol at increasing concentrations of 30%, 50% and 70% at 4°C for 5 min on a rotator. Subsequently, cells were stained *en bloc* with 3% uranyl acetate in 70% ethanol for 30 min at 4°C in the dark followed by further dehydration with increasing concentrations of 90% and 100% ethanol (3x) at 4°C for 5 min on a rotator. After dehydration, the cells were infiltrated with resin (Agar 100)/ethanol mixtures. The next day, the cells were embedded in Agar 100 in inverted BEEM-capsules and cured for 2 days at 60°C.

After polymerization the glass coverslip was removed from the dish by alternately placing the dishes on a heating plate of 40°C and immersing them in liquid nitrogen. Once the glass coverslip was removed, the cells were visible in the resin blocks. With a stereomicroscope, the cells of interest were located by matching them with the overview images taken with the SIM, and marked by a surrounding square using a scalpel. Next, after trimming the block, 50 nm serial ultrathin sections were cut from the marked block surface using a Reichardt Ultracut E ultramicrotome. All sections were collected as ribbons of 4-5 sections on triple slot grids (Ted Pella). Every grid was then poststained with 3% uranyl acetate in water for 10 min and Reynold's lead citrate for 2 min.

#### Transmission electron microscope:

EM images were taken by a JEOL TEM1400 transmission electron microscope equipped with an Olympus SIS Quemesa 11 Mpxl camera. To identify the cell of interest, low magnification (100x) EM views were compared with DIC images of the target cell and the surrounding cells, taken before EM-preparation. Once found, the cell was imaged at low magnification (1000x) and higher magnification (12kx) of the organelles of interest in every section.

#### Correlation:

Light- and electron microscopic images were correlated by overlaying one Z-plane of the EM serial images with one Z-plane of the fluorescence images. Matching of Z-planes was based on the fluorescent fiducial markers LAMP1-mCherry for lysosomes or MitoTracker for mitochondria. The LM- and EM-images were scaled and aligned using GIMP, and employing the same fiducial markers.

### **In vitro phosphorylation**

GST-PSEN2 constructs were eluted (end-over-end, 10 min, 4°C) with 2X 1 volume elution buffer (3.5 mM reduced glutathione - across organics; 50mM TrisHCl pH8.0) and 1 volume supplemented elution buffer (3.5 mM reduced glutathione; 150mM NaCl; 5 μM CaCl<sub>2</sub> 0.1% β-ME; 50mM TrisHCl pH8.0). Elutions were pooled and dialyzed (4 °C; O/N) against 250 volumes of storage buffer (5% glycerol; 1mM DTT; 20mM TrisHCl pH7.5). Substrates were concentrated (Vivaspin, 10 kDa cutoff, Millipore) and frozen until further use.

Protein kinases used (Aurora A; PKA; Cdk2; CKI; CKII) were expressed and purified in house.

*In vitro* kinase assays were as follows: bacterially expressed and purified substrate (2 µg, unless stated otherwise) was incubated with excess active kinase for 1 h at 30°C ([ $\gamma$ -<sup>32</sup>P]-ATP (0.2 µCi; 3000 Ci/mmol; Perkin-Elmer Easytides); 100 µM ATP; 2 mM MgAc; 0.05 mg/ml BSA; 1 mM DTT; 20 mM TrisHCl, pH7.5). Control reactions lacked the purified kinase or substrate. Reactions were halted with 10 mM EDTA (10 min, room temperature) and boiled in Laemmli buffer. Proteins were separated via SDS-PAGE. Phosphorylation and overall protein content was visualized by autoradiography (Typhoon FLA 9500) and blue-silverstain (Candiano et al., 2004), respectively.

#### **Tandem Mass Spectrometry (MS/MS)**

Affinity-purified GST-PSEN2 not eluted from the beads was subjected to an *in vitro* phosphorylation, as described in the corresponding section except that no [ $\gamma$ -<sup>32</sup>P]-ATP was used, followed by on-bead trypsin digestion. The resulting peptide mixture was desalted by C18 ZipTip pipette tips (Millipore) and loaded on a LC-Q Exactive Orbitrap (Thermo Fisher Scientific) MS system. Data analysis was executed by using the MASCOT (Matrix Science) search engine together with the Proteome Discoverer 1.4 PhosphoRS 3.0 workflow. The phosphorylation site assignment was also manually verified.

#### **Plasma membrane sheets preparation**

For plasma membrane sheets from MEF dKO double rescued with GFP-PSEN1 and TagRFP-PSEN2 were prepared as previously described (Chaney and Jacobson, 1983). Briefly, cells were grown to 60-70% confluency on glass coverslips were washed twice with PBS<sup>+/+</sup>, then washed with coating buffer (CB: 20 mM MES, 135 mM NaCl, 0.5 mM CaCl<sub>2</sub>, 1 mM MgCl<sub>2</sub>, pH 5.5) on ice. Cells were incubated subsequently with 1% cationic colloidal silica beads in CB and with 1mg/ml polyacrylamide in CB to coat the apical membranes (each for 1 min). After three washes with CB, cells were incubated with hypotonic buffer (2.5 mM imidazole, pH 7.0, supplemented with EDTA-free PI) for 10 min. To prepare plasma membrane sheets, shear force was applied on the coverslip using a syringe with a blunt tip needle held in a 30° angle (with respect to the coverslip). Plasma sheets were fixed for 15 min in 4% paraformaldehyde at 4°C and mounted on slides with Mowiol.